

**WETTABILITY OF SMOOTH AND ROUGH SURFACES OF  
PERFLUOROACRYLATE COPOLYMERS**

by  
EREN ŞİMŞEK

Submitted to the Graduate School of Engineering and Natural Sciences  
in partial fulfillment of  
the requirements for the degree of  
Master of Science

Sabancı University  
Summer 2006

© EREN ŐİMŐEK 2006

All Rights Reserved

To my little niece Eylül...

## ABSTRACT

In this study, it was primarily shown that random copolymers of perfluoroacrylates can have sufficient hydrophobicity to be effectively employed for the production of ultrahydrophobic surfaces via electrospinning. Presence of small molar amounts of perfluoroacrylate in the copolymer chain resulted in the formation of rather hydrophobic copolymers surfaces that had lower surface free energy than poly(tetrafluoroethylene) due to the orientation of fluorinated groups to the solid-vapor interface on the outermost surface layer. The surface energy measurements of the copolymers indicated that amphiphilic copolymers may have lower surface free energy than the copolymers of perfluoroacrylates with non-polar monomers due to the higher excess of the fluorinated groups on the surface. However, it was also shown for the ultrahydrophobic surfaces of amphiphilic copolymers that reorientation of polar groups to the solid-liquid interface due to water contact on the protrusion tops, where the long interval solid-liquid contact took place, can increase the threshold water sliding angle on the surface remarkably while the high advancing contact angles were maintained for long days. The former was detected to be a direct result of the enhanced adhesive bonds between the three phase contact line and the tops of the solid protrusions, which prevented the receding of the drops; while the latter was attributed to the preserved composite surface structure by the inability of water in penetrating through the hydrophobic walls of the cavities. Consequently, ultrahydrophobicity was lost while superhydrophobic character was preserved. This result one more time showed that high advancing contact angle values do not indicate water repellence all the time.

Due to the stability of the styrene-perfluoroacrylate copolymer surface against water exposure, this polymer was chosen to study for further improvements such as enhancing the ultrahydrophobic character. Experiments showed that the effect of applied voltage in electrospinning on the water repellence of surfaces electrospun at low solution concentrations is remarkable. By increasing the applied voltage to high values, a surface on which the microtopology was composed of nanometric beads covering the micron level roughness everywhere was produced. The resultant surface showed no

contact angle hysteresis and was perfectly non-wetting, and exhibited no adhesion with water while a pendant drop was made to touch and retreat from the surface.

## ÖZET

Bu çalışmada öncelikle gösterilmiştir ki, perfloroakrilatların gelişi güzel tekrarlanan kopolimerleri elektrodokuma ile ultrahidrofobik yüzey üretiminde etkili olarak kullanılacak yeterlikte hidrofobik karaktere sahip olabilirler. Florlu grupların en dıştaki yüzey tabakasında katı-gaz arafazına yönelmesi nedeniyle, polimer zincirinde çok az miktarda perfloroakrilat bulunması dahi tetrafloroetilenden daha düşük serbest yüzey enerjisine sahip, oldukça hidrofobik kopolimerler oluşmasıyla sonuçlanmıştır. Kopolimerlerin yüzey enerji ölçümleri göstermiştir ki yüzeylerindeki florlu grupların daha fazla olabilmesi nedeniyle amfifilik kopolimerlerin serbest yüzey enerjileri, perfloroakrilatların apolar monomerlerle yaptıkları kopolimerlerinkinden daha düşük olabilmektedir. Ancak bu amfifilik kopolimerlerin ultrahidrofobik yüzeylerinde, micro çukurlukların tepe yüzeyinde su ile uzun süreli temas sonucunda, polar grupların katı-sıvı arafazına tekrar yönelmesi ile yüzeylerin minimum su kayma açıları oldukça artmış, ancak su ile yüksek temas açılarının günlerce korunduğu gözlemlenmiştir. İlki, üç fazlı temas çizgisi ile çukurluk tepelerinin arasındaki güçlenmiş çekici bağların direk sonucu olarak damlaların geri çekilememesi; ikincisi ise suyun hidrofobik olan çukur duvarları boyunca içerilere kadar girememesi sonucu kompozit yüzey yapısının korunmuş olmasına bağlanmıştır. Özet olarak, ultrahidrofobik özellik yok olurken süperhidrofobik karakter korunmuştur. Bu sonuç bir kez daha göstermiştir ki, yüksek temas açıları her zaman su iticilik anlamına gelmemektedir.

Sitren-perfloroakrilat kopolimer, su temasına karşı dayanıklı olması nedeniyle ultrahidrofobik özellikleri daha da artırma gibi geliştirme çalışmaları yapmak için seçildi. Deneysel göstermiştir ki, düşük konsantrasyonlu solusyonlarla elektrodokumada uygulanan voltajın su iticiliğe etkisi dikkate değerdir. Uygulanan voltaj yüksek değerlere çıkarıldığı zaman mikro seviyedeki pürüzlerin üzerinde her yerin nanometrik topçuklarla kaplı olduğu bir topografya elde edildi. Bu yüzeyin, temas açısı histeresisi

göstermediđi, ve ıslanmazlıđının kusursuz olduđu görüldü, ve de asılı bir su damlası yüzeye dokundurulup çekilirken herhangi bir yapışma göstermediđi gözlemlendi.

## ACKNOWLEDGMENTS

I would like to express my gratitude for my thesis advisor Dr. Yusuf Z. Mencelođlu; first of all for his never ending belief in my academic potential and invaluable guidance throughout my whole research career at Sabanci University. Besides his academic insight, with his humanist personality and constructive style of approach to the matters, he will always be a model scientist for me.

I would like to acknowledge Dr. Kazım Acatay for teaching me most of the laboratory techniques I know today and having me drawn in my current field of study.

My professors have great contribution to the formation of this thesis. I thank Dr. Ali Rana Atılđan, Dr. Canan Atılđan, Dr. Mehmet Ali Glgn, Dr. Cleva Ow-Yang, Dr. Melih Papila and Dr. Alpay Taralp not only for conveying their priceless knowledge during the courses but also for their time and creative ideas during the discussions on my thesis project.

Without my dear friends Aylin Aydın, Ayça esmelioglu, Onur Gke, Kerem Gren, zgr Gl, Emre Heves, Burcu Karahan, Volkan Kaya, Burcu Kktrk, Iřıl Nalbant, Pınar nal, Irmak Sirer, Deniz Turgut and Sinan Yrdem, writing this thesis would not be as enjoyable as it was. I thank Iřıl also for her assistance with the drawings and formatting, and Burcu Karahan for her overall support during writing the thesis. I also thank Mustafa Cengiz nder and İbrahim İnan for their significant contribution to the project with their intense experimental work.

Last, but not least, I am grateful to my family, for their constant understanding and moral support, for their belief and respect to my academic life, and for their strong trust in my personality throughout my whole life.

## TABLE OF CONTENTS

1.	INTRODUCTION .....	1
1.1	The Origin of Surface and Interfacial Tensions.....	1
1.2	Theory of Roughness Induced Hydrophobicity .....	2
1.3	Superhydrophobic and Ultrahydrophobic Surfaces .....	6
1.4	Ultrahydrophobic Surfaces by Electrospinning .....	8
1.5	Fluorinated polymers as low surface energy solids .....	11
1.6	Purpose of the study.....	14
2.	EXPERIMENTAL.....	15
2.1	Materials .....	15
2.2	Copolymer synthesis.....	16
2.3	Characterization of the copolymers .....	16
2.4	Film preparation.....	17
2.5	Surface Characterization.....	17
2.5.1	Atomic Force Microscopy .....	17
2.5.2	SEM imaging .....	18
2.5.3	Wettability Analysis .....	18
2.5.4	Electrospinning .....	19
3.	RESULTS AND DISCUSSION .....	20
3.1	Bulk Characterization of the copolymers .....	20
3.2	Surface properties of the copolymer smooth films.....	21
3.2.1	Roughness analysis .....	21
3.2.2	Surface free energy of the copolymer surfaces.....	24
3.2.3	Dynamic contact angle analysis of the smooth copolymer films .....	26
3.2.4	Reorientation of polar groups to the surface due to water exposure ...	27
3.3	Surface properties of the rough copolymer surfaces .....	28
3.3.1	Electrospinning of the copolymers .....	28

3.3.2 Dynamic contact angle analysis of the electrospun copolymer surfaces.....	30
3.3.3 Effect of surface reorientation due to water exposure on electrospun films.....	31
3.3.4 Improving the non-wetting of the reorganization-resistive surfaces .....	39
4. CONCLUSION.....	45
REFERENCES .....	47

## LIST OF FIGURES

<b>Figure 1.1</b> Attractive forces acting on liquid molecules in bulk and at the surface .....	1
<b>Figure 1.2</b> Schematic representation of a liquid deposited on a solid surface .....	2
<b>Figure 1.3</b> Advancing of the TPCL when water is added to drop (left) and receding of the TPCL when water is withdrawn from the drop (right) .....	3
<b>Figure 1.4</b> Schematic representation of a liquid in a Wenzel state .....	5
<b>Figure 1.5</b> Schematic representation of a liquid in a Cassie-Baxter state .....	6
<b>Figure 1.6</b> Schematic representation of surface with two different roughness topologies. The darker lines show the possible TPCLs for a water drop in contact with the surfaces. (a) a surface on which a fairly continuous contact line can form (b) separated posts on which a very discontinuous contact line can form .....	7
<b>Figure 1.7</b> A bead-only (A), bead on the string (B) and fiber-only (C) surface generated by electrospinning .....	9
<b>Figure 1.8</b> A typical electrospinning setup .....	9
<b>Figure 2.1</b> Chemical structures of the monomers used for copolymer synthesis..	15
<b>Figure 3.1</b> AFM images (5x5 $\mu\text{m}^2$ ) of the copolymer films A) MP, B) GP, C) SP1 and D) SP2. Subscript 1 refers to solution casting and 2 refers to dip coating. Vertical scales are 10 nm for A <sub>1</sub> , B <sub>1</sub> and C <sub>1</sub> ; 40 nm for D <sub>1</sub> and 30 nm for A <sub>2</sub> , B <sub>2</sub> , C <sub>2</sub> and D <sub>2</sub> .....	23
<b>Figure 3.2</b> Typical SEM images of the electrospun copolymer films A) MP, B) GP, C) SP1 and D) SP2. Subscript 1 represents the images at higher magnification. Scale bars correspond to 10 and 1 $\mu\text{m}$ for the left and right images, respectively. ....	29
<b>Figure 3.3</b> Sliding angles vs exposure time to water for the copolymer electrospun films MP ( $\square$ ), GM ( $\diamond$ ), SP1 ( $\Delta$ ) and SP2 ( $\circ$ ) .....	32

<b>Figure 3.4</b> Shapes of TPCLs in different states. Gray regions represent the solid surface. Blue lines represent the water molecules within the TPCL .....	34
<b>Figure 3.5</b> Physical events that occur during receding of a water drop on a smooth (up) and Wenzel (down) surface.....	35
<b>Figure 3.6</b> The change in the TPCL when pressure is applied to a drop in a metastable Cassie-Baxter state. Gray regions represent the solid surface. Blue lines represent the water molecules within the TPCL.....	37
<b>Figure 3.7</b> The state of the TPCL on the water treated electrospun MP surface. Red lines show the regions went under reorganization due to water exposure .....	38
<b>Figure 3.8</b> Electrospun surfaces of the SP2 copolymer at 2 w % concentration and 8 kV applied voltage. Magnifications are 5000 and 25000 for upper and lower images, respectively .....	41
<b>Figure 3.9</b> Electrospun surfaces of the SP2 copolymer at 3 w % concentration and 10 kV applied voltage. Magnifications are 5000 and 40000 for upper and lower images, respectively. This image is the same as Figure 3.2-D but put for comparison.....	42
<b>Figure 3.10</b> Electrospun surfaces of the SP2 copolymer at 2 w % concentration and 11.5 kV applied voltage. Magnifications are 5000 and 25000 for upper and lower images, respectively.....	43
<b>Figure 3.11</b> Electrospun surfaces of the SP2 copolymer at 2 w % concentration and 15 kV applied voltage. Magnifications are 5000 and 25000 for upper and lower images, respectively.....	44

## LIST OF TABLES

<b>Table 3.1</b> Bulk characteristics of the copolymers.....	20
<b>Table 3.2</b> Roughness parameters for the cast films <sup>a</sup> .....	22
<b>Table 3.3</b> Water, ethylene glycol and n-hexadecane advancing contact angles of the dip coated films and surface free energies .....	24
<b>Table 3.4</b> Dynamic contact angle analysis of the dip coated films .....	26
<b>Table 3.5</b> Dynamic contact angle analysis of the as produced electrospun films	31
<b>Table 3.6</b> Dynamic contact angle analysis of the electrospun films after 11 days of water exposure.....	32

## 1. INTRODUCTION

### 1.1 The Origin of Surface and Interfacial Tensions

The surface and interfacial tensions phenomena are readily explained by the short-range forces of attraction between the molecules. For instance, as represented in Figure 1.1, the molecules located at the bulk of a liquid are subjected to equal attractive forces in all directions. However, the ones located at the liquid-vapor interface are unbalanced and they cause a net inward pull. This net force cause as many molecules as possible to leave the surface and transfer to the bulk, causing the surface to contract spontaneously. Consequently, liquid drops tend to attain a spherical shape that also minimizes the surface area thus the total surface tension [1].

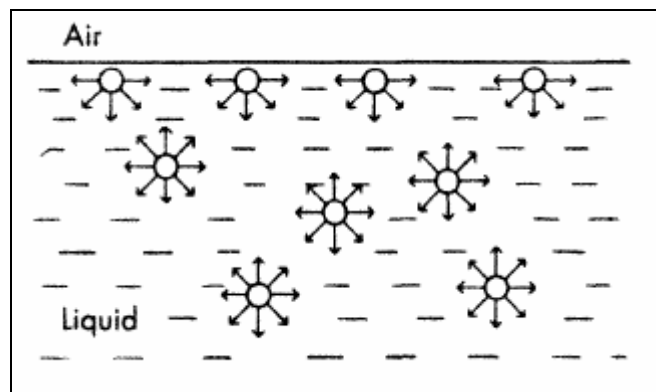


**Figure 1.1** Attractive forces acting on liquid molecules in bulk and at the surface [1]

In general, surface tension is the force per unit length, and may equally be thought as free energy per unit area, i.e. *surface free energy*. In general, polar molecules like water have strong intermolecular forces, so the net force at the surface is high and

they have high surface energy. Non-polar molecules, such as fluorocarbons, have however weak intermolecular forces and corresponding low surface energies.

## 1.2 Theory of Roughness Induced Hydrophobicity

In general, if a liquid is placed on a solid surface, it does not wet the surface completely (a complete spreading out case) but it remains as a drop which has a definite angle of contact at the solid-liquid interface as shown in Figure 1.2.

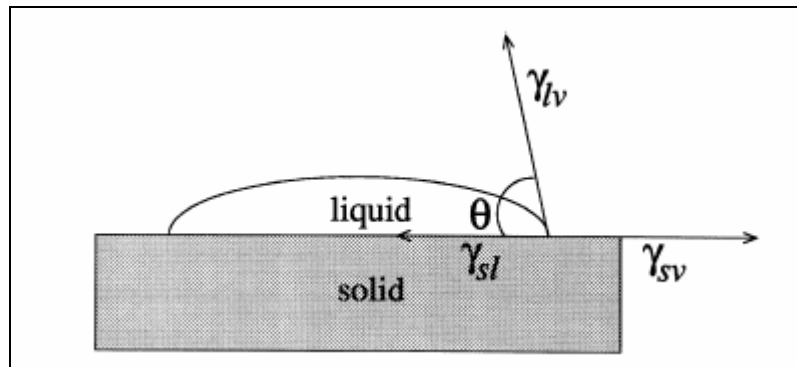


**Figure 1.2** Schematic representation of a liquid deposited on a solid surface [2]

In such a situation, the drop is in mechanical equilibrium under the action of the three interfacial tensions: solid-vapor ( $\gamma_{sv}$ ) solid-liquid ( $\gamma_{sl}$ ) and liquid-vapor ( $\gamma_{lv}$ ). This equilibrium relation determines the contact angle ( $\theta$ ) at the contact point where the intersection of the three phases occurs and given by the Young's equation as [3]:

$$\cos \theta = \frac{\gamma_{sv} - \gamma_{sl}}{\gamma_{lv}} \quad (1)$$

It should be kept in mind that this equation assumes a smooth surface on which the phases are mutually in equilibrium and the contact angle is called the *equilibrium contact angle*. Experimentally accessible contact angles may or may not be equal to the

$\theta$  in Young's equation. This point will be discussed later. According to Equation 1, if the free energy of the dry solid,  $\gamma_{SV}$ , is lower than that of the wet solid,  $\gamma_{SL}$ , the water contact angle occurs to be greater than  $90^\circ$  and the surface is termed as hydrophobic. Although Equation 1 predicts contact angles up to  $180^\circ$ , the situation is practically limited and the highest reported water contact angle on a smooth surface is  $122^\circ$  [4].

The equilibrium contact angle in Equation 1 is in fact a unique (theoretical) contact angle. However, if more liquid is added to a water in equilibrium with the surface, the contact angle first increases to a maximum value referred as the *advancing contact angle* ( $\theta_a$ ), and then remains unchanged by the advancing of the *three phase contact line* (TPCL), which is formed by the liquid molecules at the intersection of the solid-liquid, solid-vapor and liquid-vapor interfaces. On the other hand, if liquid is withdrawn from the drop by inserting a needle, the contact angle first decreases to a minimum value referred as the *receding contact angle* ( $\theta_r$ ), and then remains unchanged by the retreating of the TPCL. The difference between  $\theta_a$  and  $\theta_r$  is referred as the *contact angle hysteresis* ( $\Delta\theta$ ). Figure 1.3 shows the schematic representation of the events occurring during the advancing-receding process.

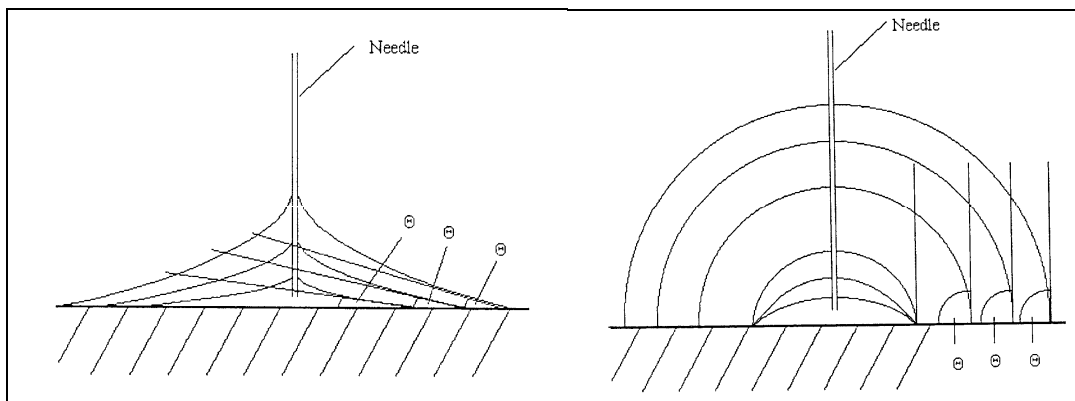


**Figure 1.3** Advancing of the TPCL when water is added to drop (left) and receding of the TPCL when water is withdrawn from the drop (right)

The contact angle hysteresis is often attributed to chemical heterogeneities or roughness. In theory, ideal solid surfaces do not show contact angle hysteresis. However, in the absence of heterogeneities or roughness, nearly all of the surfaces display measurable hysteresis, which arises from the adhesive bond between the liquid

and solid during spreading [5-8]. Consequently, movement of a TPCL requires an activation energy to break this adhesive bond that is macroscopically expressed as drop distortion [9]. In other words, in fact we witness the advancing and receding contact angles on the front and rear sides (in the direction of motion) of a distorted rain drop which slides on a window glass.

In the hydrophobicity literature, there are numerous studies reporting the wettability of a surface with just a single stationary contact angle. However, any stationary contact angle, which is between the advancing and receding contact angles, can be observed for a drop sitting on a solid surface. Thus, advancing and receding contact angles are of great importance and can be denoted as intrinsic properties for characterizing the wetting properties of a solid surface instead of stating a less meaningful stationary contact angle [9-12]. Another interpretation of the contact angle hysteresis is the minimum force ( $F$ ) needed to start a drop moving over a solid surface and given by the equation [13]:

$$F = \frac{mg(\sin \alpha)}{w} = \gamma_{LV}(\cos \theta_r - \cos \theta_a) \quad (2)$$

where  $g$  is the acceleration due to gravity, and  $m$  and  $w$  are the mass and width (horizontal to the movement direction) of the drop, respectively.  $\alpha$  in Equation 2 is termed as the *sliding angle*, which is the threshold tilting angle at which a drop starts to move on a surface. Thus, sliding angles can be used effectively to monitor the contact angle hysteresis; however, this would be a less general characterization method in terms of wettability because sliding event is a function of drop size and is limited to surface on which drops do not stick.

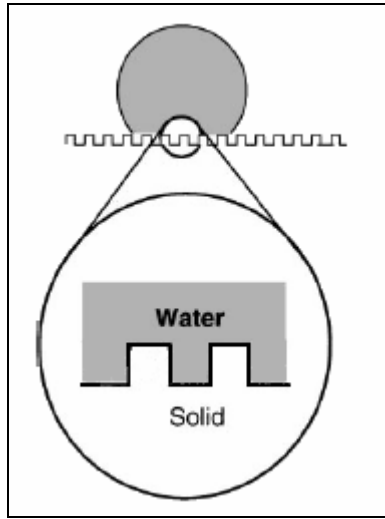


**Figure 1.4** Schematic representation of a liquid in a Wenzel state

On rough solid surfaces, where there is a continuous solid-liquid interface by the penetration of the liquid into the grooves completely, as shown in Figure 1.4, Wenzel [14] suggested that, the *apparent contact angle* ( $\theta^*$ ) would be related to the Young's contact angle  $\theta$ , with the ratio of the actual surface area over the projected surface area ( $\sigma$ ) as following:

$$\cos \theta^* = \sigma \cos \theta \quad (3)$$

Wenzel equation predicts that if the surface is hydrophilic ( $\theta < 90^\circ$ ), then the roughness should enhance wetting and if the surface is hydrophobic, the contact angle of the rough surface should be more than that on the smooth surface.

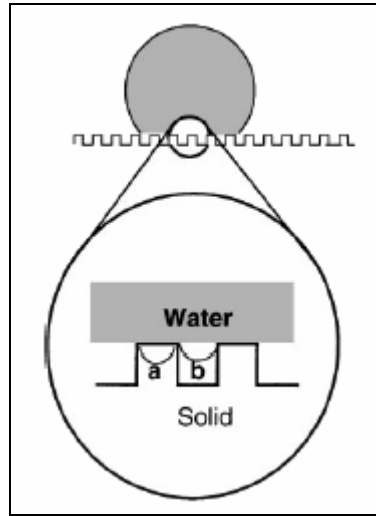


**Figure 1.5** Schematic representation of a liquid in a Cassie-Baxter state

Another regime, referred as a *composite* surface, was described by Cassie and Baxter [15] for rough surfaces, which corresponds to the state that the fluid sits on the protrusions and trapped air between them as shown in Figure 1.5. For such a condition, the apparent contact angle is related to the Young's angle as:

$$\cos \theta^* = f_1 \cos \theta + (1 - f_1) \cos 180 \quad (4)$$

where  $f_1$  and  $f_2$  are the fractions of the liquid in contact with solid and air, respectively. Johnson and Dettre [16] showed that a transition from a Wenzel to Cassie-Baxter state occurs if the surface roughness reaches a critical level (for a hydrophobic solid). This transition is characterized macroscopically by high static contact angle values and particularly with a relative decrease in the hysteresis [10-12].

### 1.3 Superhydrophobic and Ultrahydrophobic Surfaces

The Cassie-Baxter phenomenon has gained more attention by the investigation of the hydrophobic, rough ever clean Lotus leaf, when it was observed that drops running off the leaf surfaces clean the surface by carrying the contaminants [17]. After the

identification of this *self cleaning* mechanism by its relation with the composite surface structure, considerable efforts have been made to mimic the topography of the Lotus surface and numerous methods have been reported to achieve *superhydrophobic* surfaces which are characterized by apparent contact angles greater than  $150^\circ$ .

When designing superhydrophobic surfaces, the main process is either introducing roughness on the surface of a hydrophobic solid or decreasing the surface free energy of a rough surface with a hydrophobic coating. In both of the cases, the surface should be hydrophobic and sufficiently rough so that air pockets are favored under the drop instead of penetration into the cavities. In other words, superhydrophobicity is possible only through a composite surface. However, not all of the superhydrophobic surfaces are non-wetting or self-cleaning since Equation 2 predicts that, drops can slide only on surfaces exhibiting low contact angle hysteresis. For this, Chen et al. described the surfaces on which water drops can move easily as *ultrahydrophobic* [11]. The main point in this discussion is that superhydrophobicity is defined within a single, stationary contact angle, on the other hand, TPCL can be rather stable on a superhydrophobic surface because of the physical structure of the roughness [10-12]. For instance, Chen et al. in reference 11 discussed the wetting properties of two superhydrophobic surfaces with two different roughness topologies represented in Figure 1.6:

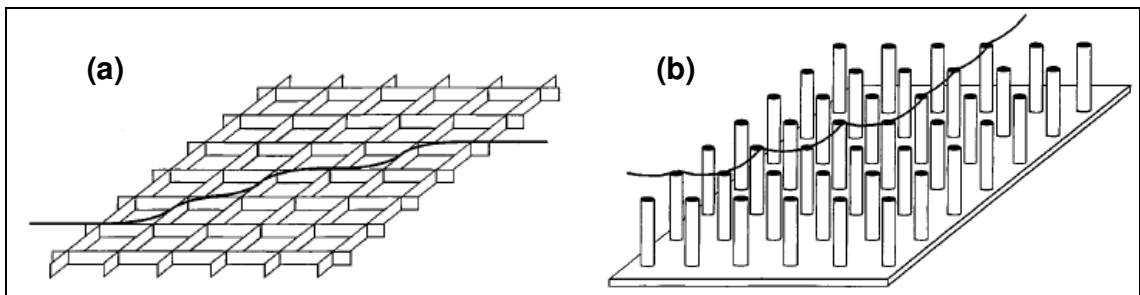


**Figure 1.6** Schematic representation of surface with two different roughness topologies. The darker lines show the possible TPCLs for a water drop in contact with the surfaces. (a) a surface on which a fairly continuous contact line can form (b) separated posts on which a very discontinuous contact line can form [11]

These two surfaces are designed so that the fractions of the open areas ( $f_2$  in Equation 4) are same and equal to 99 % for both surfaces. If both of these surfaces are coated with poly(tetrafluoroethylene) (PTFE, contact angle  $\sim 110^\circ$ ), Equation 4 predicts that the apparent water contact angle should be  $173^\circ$ . However, the dynamic wettability

of the surfaces should be completely different. It would be worth noting that the only solid-liquid interfacial water molecules that move when a drop moves on a surface are the ones on the TPCL. As discussed before, movement of the contact line requires an activation energy due to the adhesive bond between the solid and water at the contacting regions of the TPCL. So the amount of contact per unit length for TPCL would be high if the roughness is very continuous as it is on the surface in Figure 1.6-a. So this would require a higher activation energy barrier and the TPCL would be relatively stable. Thus, hysteresis would be high and the drop would stick to the surface. However, if the surface roughness is in the geometric shape described in Figure 1.6-b, the TPCL cannot make continuous contact with the surface and is rather long. So the energy barriers are low and the TPCL can move without the need of much energy. Consequently, low hysteresis is observed and drops can roll-off the surface easily. Although both surfaces are superhydrophobic, the one in Figure 1.6-b is ultrahydrophobic and self cleaning.

#### **1.4 Ultrahydrophobic Surfaces by Electrospinning**

Section 1.3 summarizes that, in the design of non-wetting surfaces, the consideration of the possible TPCLs should also be made. Thus, methods which result surfaces having fairly discontinuous roughness in terms of micro-topology are of quite significance for ultrahydrophobicity. One of the methods for generating ultrahydrophobic surfaces is electrospinning which was reported to be very effective for creating polymeric surfaces composed of isolated micro spheres (beads) that are very rough and discontinuous in three dimensions [18-23]. In addition, more continuous, micron and sub-micron fibers can also exhibit ultrahydrophobicity but the threshold sliding angles on fibered surfaces are higher than those of the beaded surfaces [24, 25]. Figure 1.7 shows examples of surfaces generated by electrospinning.

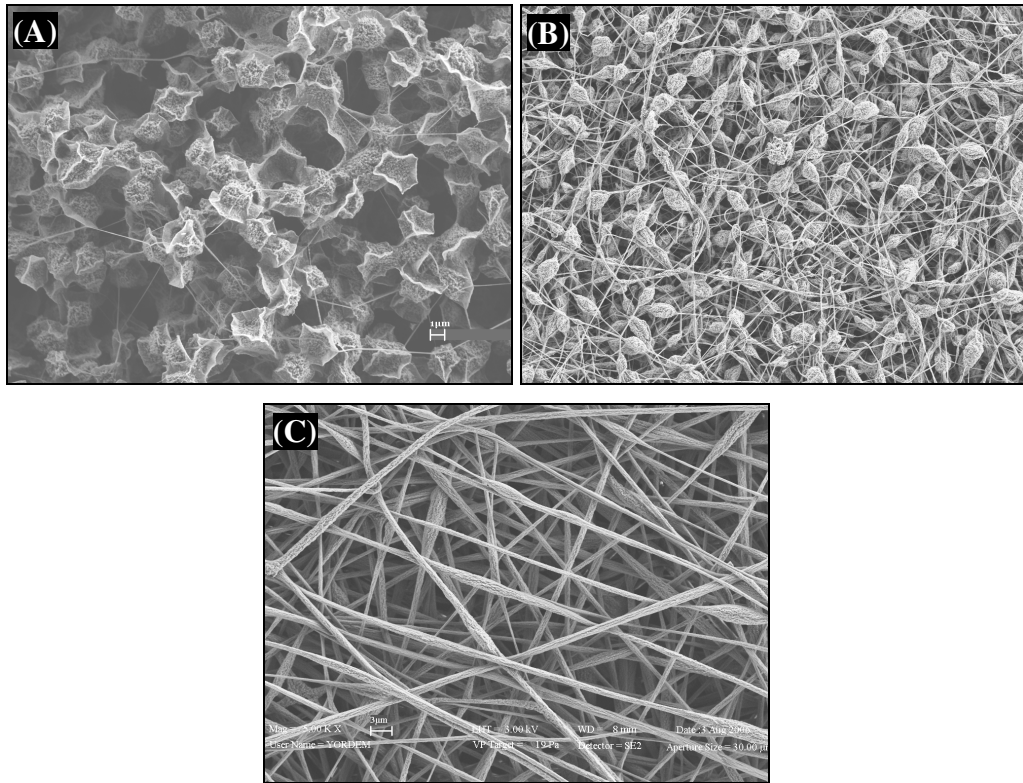


**Figure 1.7** A bead-only (A), bead on the string (B) and fiber-only (C) surface generated by electrospinning

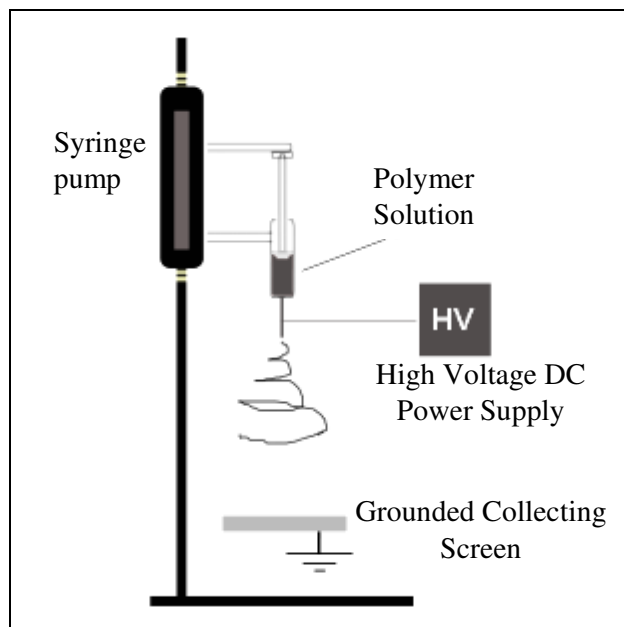


**Figure 1.8** A typical electrospinning setup

Electrospinning has been used mainly for the production of fibers in the sub-micron and nanometer diameter range. A typical electrospinning process is composed of a high voltage supply, a grounded collecting screen and an optional syringe pump may be equipped for controlling the process more effectively. A representative setup is shown in Figure 1.8. If a high static voltage, usually between 8 and 40 kV, is applied to the metal tip of the syringe, an electrical force in the direction from tip to grounded screen occurs while the polymer solution (or melt), which is held by its surface tension at the tip of the syringe, is charged. Mutual charge repulsion causes an electrical force opposite to the surface tension [26]. If the intensity of the electrical field is increased, the hemispherical shape of the solution at tip is distorted by the increasing force and a Taylor cone is formed [27]. When the electrical force overcomes the surface tension, a jet of solution with a diameter in the range of 10 to 100  $\mu\text{m}$  is ejected from the tip of the Taylor cone. An electrically driven bending instability grows at the tip of the jet while the jet becomes longer and thinner that makes the jet follow a spiraling loop [28]. Meanwhile, the jet solidifies and dry fibers, as shown in Figure 1.7-C, are formed on the grounded screen.

The versatility of the process comes from that a huge range of polymers can be electrospun and surfaces of various microtopologies can be achieved by tuning the process parameters. The main parameters for electrospinning can be divided into two groups, solution properties such as viscosity, elasticity, conductivity and surface tension, and setup parameters such as applied voltage and tip to ground distance. Among these parameters, solution viscosity has important impact on the final film structure. For instance, fiber diameter is very sensitive to solution viscosity which is normally an increasing function of the concentration for a fixed polymer molecular weight, solvent and ambient temperature. The general trend in electrospinning is that increasing solution concentration amplifies fiber diameter and some mathematical relation can be found between fiber diameter and concentration [29, 30]. However, the formation of the fibers are limited to a fixed viscosity range for a certain system (i.e. certain polymer and solvent type with other parameters fixed) [26]. For instance, at relatively low concentrations, beads strung along the fibers can form, and further decrease in concentration can even lead to isolated beads [18].

Another important parameter affecting the final film structure during electrospinning is applied voltage. The effect of voltage is in favor of decreasing the fiber diameter. However, it may be less than that of the solution concentration; but the morphology of the fibers is greatly influenced by the applied voltage. There is an important low limit for the applied voltage since electrospinning would not be possible below voltage values which are not sufficient for ejection of the jet due to electrical forces.

The flexibility of electrospinning brings out that the degree of superhydrophobicity and ultrahydrophobicity can be easily tuned via engineering the physical properties of the electrospun films by changing the corresponding parameters [18]. However, it is important to recall that the other requirement of the composite surface formation is a low surface energy solid, which should be a hydrophobic polymer.

### **1.5 Fluorinated polymers as low surface energy solids**

Because of their low surface energy characteristics, application of fluorinated materials for the production of superhydrophobic and ultrahydrophobic surfaces, as either coating for rough surfaces or as the hydrophobic solid itself to be roughened, is common. If the microtopologic requirements are met, fluorinated polymers can be used extensively for this purpose. The surface free energy of a solid depends on the chemical composition of the surface and decreases for fluorocarbons in the order of  $-\text{CF}_2\text{H}$ ,  $-\text{CF}_2-$  and  $-\text{CF}_3$ , respectively [31, 32]. It has been shown in many reports that homopolymers of fluorinated acrylates and siloxanes, or their copolymers with conventional monomers can show very low surface free energy since the fluorinated chains orient towards the solid-air interface in order to decrease the surface free energy [33-44]. Particularly for the copolymers of perfluorinated (pendant chain) monomers, the outermost layer of the polymers are covered with a large concentration of the fluorinated segment, which differ remarkably from the bulk composition, and their  $-\text{CF}_3$  end group plays a key role for minimizing the surface free energy. Consequently, they stand as good substitutes for

the hard-to-process and expensive fully fluorinated polymers such as PTFE which has become the point of reference low surface energy material.

As mentioned in section 1.1, surfaces exhibit a tension as a result of unbalanced intermolecular forces at the surface. This requires that, all surfaces are energetically unfavorable because they have positive free energy of formation. This phenomenon can be understood easily if the formation of a surface is considered in terms of energetics of bond breaking. When a new surface is to be formed by the cleavage of a solid, bonds have to be broken between the molecules on either side of the cleavage plane, so work is done on the system. Thus, the surface free energy (surface tension) contribution to the total free energy of a system must be positive. Consequently, formation of a surface is not favored. However, total free energy of the surface may be minimized in several ways, such as reducing the amount of surface area exposed, exposing low surface energy segments or changing the local surface geometry in favor of low surface energy. The first and last points are much more limited to liquids, metals and crystal structures. Polymers which usually contain several constituents of various surface energies, on the other hand, can lower their surface free energy by enriching the surface with the lower energy segments. This phenomenon was put forward by two theories. Firstly, according Gibbs adsorption law, the surface concentration of a molecule can differ from the bulk according to the equation [36, 45]:

$$\Gamma_i = - \frac{d\gamma}{d(\ln C)} \times \frac{1}{(nRT)} \quad (5)$$

where  $\Gamma_i$  is the surface excess of a species  $i$  for two components system in mols per unit area of surface,  $C$ ,  $R$ ,  $T$  and  $n$  are the concentration of species, the ideal gas constant, temperature and the correction factor depending on the nature of the surface molecule considered, respectively. The summary of this equation is that if  $d\gamma / d(\ln C) < 0$ , in other words, if the surface energy has a decreasing trend with a species, then there would be excess of these species on the surface. Second theory of our interest is the Langmuir's *law of surface action* [46]. According to this law, the surface energy is the sum of the local surface free energies [34] such that:

$$\gamma = r_1\gamma_A + r_2\gamma_B \quad (6)$$

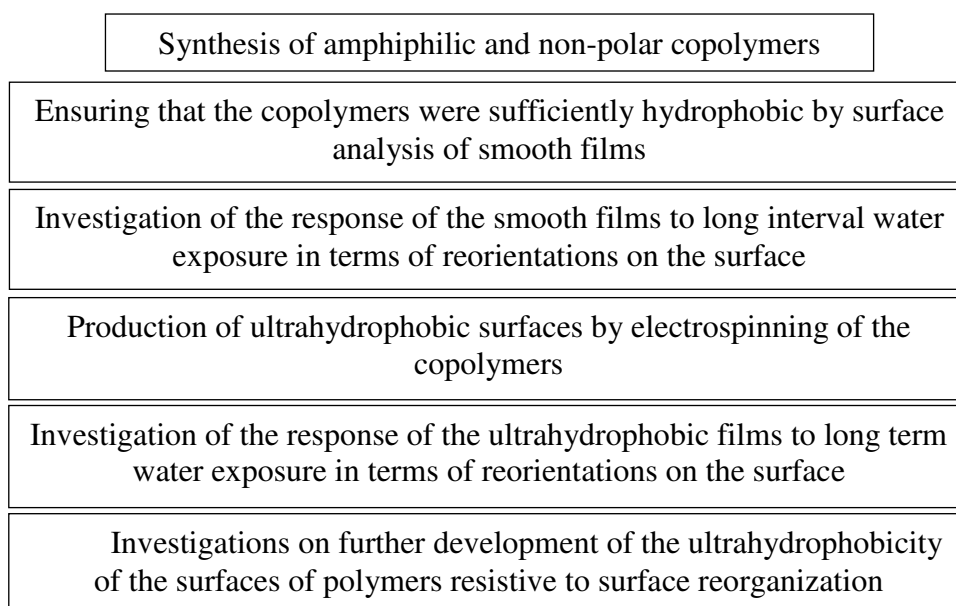
where  $r_1$  and  $r_2$  are the fractions of surface covered by A and B, respectively, for a surface consisting of A and B. These two equations (Equations 5 and 6) clearly predict that the outermost layer of the fluorinated copolymers would be composed of mostly with the lowest surface energy, fluorinated groups. Particularly, the contribution of the  $-\text{CF}_3$  end group for perfluorinated pendant chains to the total surface energy would be of great significance. Thus, very small molar amounts of perfluoroacrylates in the copolymer would lead to very low surface energies even if the other monomer has polar groups [33, 36, 37, 44]. However, this property may have some drawbacks at the same time, since it would be comprehensible that in polar environments (i.e. high humidity, water exposure) the polar groups this time tend to orient to the surface to decrease the interfacial energy and the wettability of the surface increases.

Except for several studies [33, 36, 44], random copolymers of perfluorinated acrylates have been of less interest. This is mainly due to that the low surface energy properties of fluorinated polymers also depend on the degree of ordering of the pendant chains (the higher the order of the pendant chain, the more  $-\text{CF}_3$  end groups directed to the surface). For instance, the liquid crystalline ordering of perfluoroalkyl side chains in the block and graft copolymers not only greatly enhances the density of  $-\text{CF}_3$  end groups at the interface thus minimizes the surface free energy [33, 37, 38, 44, 47], but also makes the surface more resistive to reorientation of the low surface energy groups to the interface due to polar environment [38, 42, 48]. However, perfluoroacrylate random copolymers can have comparable low surface free energy and hydrophobic properties; and with their good solubility in organic solvents, they have the potential to be used for the production of ultrahydrophobic surfaces by electrospinning. The overall process would be easy, versatile and cheap in means of both the production of the copolymers (a basic solution polymerization can be employed) and their transfer into ultrahydrophobic surface by electrospinning, which was discussed in Section 1.4. In addition, although the movement of polar groups to the surface due to polar environment can limit the applications of this kind of copolymers, for a composite surface of minimized solid-liquid interface, this phenomenon may be less effective or more time dependent since reconstruction can occur only on the fractions of the surface

in contact with the new environment which will be water in this case. Such an investigation may also clarify the questions regarding the stability of the superhydrophobic surfaces of amphiphilic copolymers against exposure to water. Here, the term stability should refer to the durability of a drop in the Cassie-Baxter state. As stated in section 1.2 in detail, transformation to Cassie-Baxter from Wenzel regime can occur only for sufficiently hydrophobic and rough surfaces. However, for a surface which is rather rough but not hydrophobic enough, either the drop should be in the Wenzel regime directly or a *metastable Cassie-Baxter* state, in which the trapped air below may still be favored but an irreversible transition to Wenzel regime takes place if a pressure is applied to the drop, occurs [49].

## 1.6 Purpose of the study

In this study, because of the superior properties of the perfluoroacrylate copolymers discussed in section 1.5, the primary aim was the production of ultrahydrophobic surfaces from perfluoroacrylate copolymers by electrospinning. Then it would be possible to investigate how the bulk properties of the copolymers affect the wetting properties when a long contact with water, which can cause reorientation of polar or less hydrophobic groups from the bulk to the surface, occurs. The summary of the proposal is given in the flowchart below:



## 2. EXPERIMENTAL

### 2.1 Materials

The chemical structures of the monomers used were given in Figure 2.1. Glycidyl methacrylate (GMA, Aldrich), methyl methacrylate (MMA, Aldrich) and styrene (technical) were purified by passing through an alumina column. Perfluoroalkylethyl acrylate (PFA,  $\text{H}_2\text{C}=\text{CHCO}_2(\text{CH}_2)_2(\text{CF}_2)_n\text{CF}_3$ ),  $n =$  mixture of 6, 8 and 10, Clariant Fluowet AC812) and all reagent grade solvents, trichloroethylene (TCE, Riedel) and tetrahydrofuran (THF, Merck) and dimethylformamide (DMF, Merck), were used as received. 2,2'-azobisisobutyronitrile (AIBN, Fluka) was recrystallized from methanol and stored at  $-20\text{ }^\circ\text{C}$  prior to use.

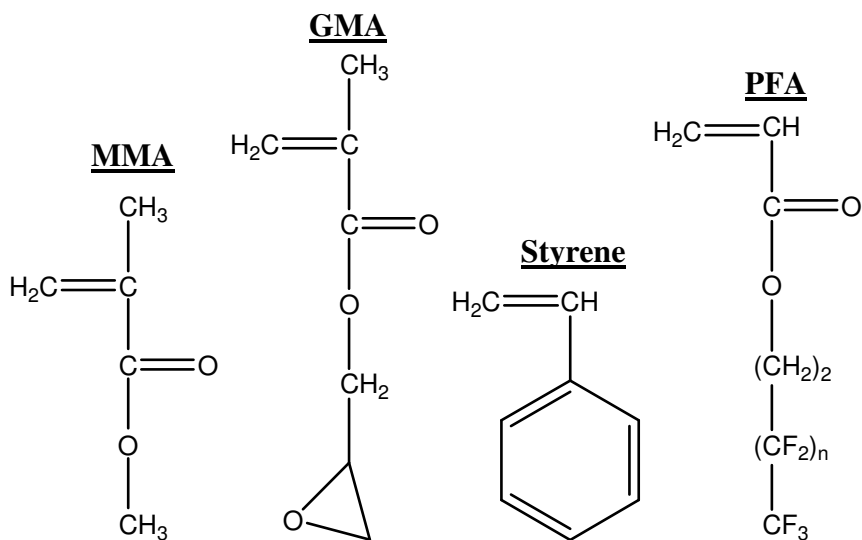


**Figure 2.1** Chemical structures of the monomers used for copolymer synthesis

## 2.2 Copolymer synthesis

Poly(methyl methacrylate-co-perfluoroalkylethyl acrylate), poly(glycidyl methacrylate-co-perfluoroalkylethyl acrylate) and poly(styrene-co-perfluoroalkylethyl acrylate) random copolymers were synthesized as 5 mol % PFA by feed and denoted as MP, GP and SP1 in short terms, respectively. An additional random copolymer of styrene with PFA, denoted as SP2, was synthesized as 10 mol % PFA by feed. For all of the polymerization, AIBN was used as the initiator at 0.04 mol % with respect to the total monomer mol in the reactor and THF was used as the solvent. Freeze and thaw cycle was performed three times for each polymerization to remove the oxygen of the media and the consequent vacuum in the reactors were broken with high purity Argon. The reactions were carried out by free radical copolymerization at 65 °C for 5 days. The pure copolymers were achieved by first precipitating in methanol, then washing with methanol several times and finally drying in a vacuum oven at 45 °C for 12 hours.

## 2.3 Characterization of the copolymers

The copolymer composition was determined by <sup>1</sup>H NMR peak integration technique by using a 500 MHz Varian Inova NMR. Deuterated THF was used as the solvent and chemical shifts were referenced to Tetramethylsilane (TMS). Molecular weight and molecular weight distributions were determined by a gel permeation chromatography (GPC) instrument, an Agilent Model 1100 consisting of a pump, a refractive index detector and four Waters Styragel columns HR 5E, HR 4E, HR 3, HR 2; and THF was used as eluent at a flow rate of 0.3 ml/min at 30 °C. Molecular weights were calibrated using poly(methyl methacrylate) and polystyrene standards.

Thermal properties of the polymers were analyzed with a Netzsch 204 Phoenix differential scanning calorimeter (DSC) by using sample masses of about 10 mg and running from -50 to 250 °C under nitrogen atmosphere at a scan rate of 10 °K/min.

## 2.4 Film preparation

For coating applications, 6 w % THF and trichloroethylene solutions of the copolymers were prepared. Solution casting of films was performed by coating 2.5 x 7.5 cm cleaned microscope slides by covering the whole slide surface. Dip coating procedure was performed by immersing 1 x 2 cm cleaned mica slides in a vertical position into trichloroethylene solutions for 5 minutes and emerging at a rate of 2 mm/min. Drying was processed by first slowly at room temperature for 24 hours and then further keeping in a vacuum oven at room temperature for 8 hours in order to assure a dry surface.

## 2.5 Surface Characterization

### 2.5.1 Atomic Force Microscopy

The surface morphologies of the solution cast and dip coated films were analyzed with an atomic force microscope (AFM), Multimode-Nanoscope IIIa, Veeco Metrology Group, Santa Barbara, CA in the tapping mode. The cantilever was made of standard silicon tip with 31.26 N/m force constant and 281.61 kHz oscillating frequency. The scan range was 50x50 and 5x5  $\mu\text{m}^2$ , and the scan speed was 1Hz. The surface roughness was evaluated by average roughness ( $R_a$ ), root-mean-square roughness ( $R_q$ ), ratio of actual over projected area ( $\sigma$ ), from the 50x50  $\mu\text{m}^2$  scans with the help of the Nanoscope (resident) software.

Asperity rise angles ( $\phi$ ) were calculated from AFM images by first differentiating the z (height) versus x data of the line scans and then converting these slopes to rise angles through the relation  $\phi = \arctan(dz/dx)$ . Overall averages and standard deviations were computed for each surface using  $\phi$  values from 9 individual line scans taken from 3 images of different regions of the same sample.

### 2.5.2 SEM imaging

SEM imaging of the electrospun films was performed on a LEO Supra VP35 FE-SEM after sputter deposition of a thin conductive carbon coating onto samples which were electrospun onto aluminum foils.

### 2.5.3 Wettability Analysis

Static and dynamic contact angle analysis of the samples was performed by using sessile drop method with a Krüss GmbH DSA 10 Mk 2 goniometer with DSA 1.8 software. In all of the measurements, freshly distilled ultrapure Milipore water was used. Advancing/receding angles were determined by measuring the contact angles at the onset of advancing/retracting of the three phase contact lines while slowly injecting/withdrawing water from the pre-deposited drops, with the help of a 1 mL syringe occupied with a micrometer. 2.5 and 25  $\mu\text{L}$  drops were deposited on the sample for advancing and receding measurements respectively, and measurements from 10 different regions were averaged. During the dynamic contact angle analysis, the tip of the syringe (0.5 mm diameter) was kept in the drops within the measurements and a tangent method, in which the part of the profile of a sessile drop lying near the baseline is adapted to fit a polynomial function, is employed to calculate the contact angles from the slope at the three phase contact point.

Surface energies of the films were calculated from advancing contact angle measurements [2] of water, ethylene glycol and n-hexadecane by using Owen, Wendt, Fowkes concept [50, 51]. This approach states that surface energy of a solid  $\gamma_{\text{SV}}$  can be broken down into a dispersive  $\gamma_{\text{SV}}^{\text{d}}$  and polar  $\gamma_{\text{SV}}^{\text{p}}$  component as:

$$\gamma_{\text{SV}} = \gamma_{\text{SV}}^{\text{d}} + \gamma_{\text{SV}}^{\text{p}}$$

and the advancing contact angle of a liquid can be related to the interfacial surface energies as:

$$\frac{1}{2} (1 + \cos \theta_a) \gamma_{\text{LV}} / (\gamma_{\text{LV}}^{\text{d}})^{0.5} = (\gamma_{\text{SV}}^{\text{p}})^{0.5} (\gamma_{\text{LV}}^{\text{p}} / \gamma_{\text{LV}}^{\text{d}})^{0.5} + (\gamma_{\text{SV}}^{\text{d}})^{0.5}$$

Through this equation, by using at least two liquids, whose surface tension and the dispersive and polar components are known, if the  $\frac{1}{2} (1+\cos \theta_a) \gamma_{LV}/(\gamma_{LV}^d)^{0.5}$  is plotted against  $(\gamma_{LV}^p / \gamma_{LV}^d)^{0.5}$  and fit to a linear equation, then the polar component of the solid-vapor interfacial energy can be calculated from the slope of the line and dispersive component can be evaluated from the y-intercept.

Threshold sliding angle measurements was performed by first depositing a 10  $\mu$ L water drop on a surface which was placed on a horizontal plate and then very slowly tilting the plate with the help of a micrometer until the drop started to move. At least ten measurements were averaged from different regions for each sample.

#### **2.5.4 Electrospinning**

Corresponding solutions of the copolymers were prepared by dissolving in 1:1 THF:DMF mixture by weight and transferred into a 2.5 mL syringe equipped with a metal tip. For maintaining a stable volume of solution on the tip of the syringe, a Univentor 801 syringe pump was used. The electrospinning setup was built by placing the syringe pump vertically by pointing the syringe tip downwards, where the grounded aluminum foil screen was kept horizontal below as shown in Figure 1.8. In all experiments, the tip to ground distance was kept constant at 10 cm, and flow rate was set according to maintain a constant amount of solution at the tip of the syringe that was kept nearly same size for all electrospinnings.

### 3. RESULTS AND DISCUSSION

#### 3.1 Bulk Characterization of the copolymers

**Table 3.1** Bulk characteristics of the copolymers

Copolymers	$M_n$	$M_w / M_n$	PFAEA content by feed	PFAEA content by $^1\text{H-NMR}$	$T_g$ ( $^{\circ}\text{C}$ )
MP	85,700	1.9	5	4.3	95.5
GP	67,500	2.7	5	5.2	65.4
SP1	89,300	1.8	5	6.8	83.2
SP2	105,600	1.8	10	13	70.7

\*  $M_n$ : number-average molecular weight (g/mol).  $M_w$ : weight-average molecular weight.  $T_g$ : glass transition temperature. PFAEA contents refer to mol %

High polydispersity index ( $M_w / M_n$ ) of the copolymers were characteristic of solution polymerization. Glass transition temperatures of the copolymers were lower than that of PMMA (105  $^{\circ}\text{C}$ ) for MP, and that of PS (95  $^{\circ}\text{C}$ ) for PS1 and PS2, which can be attributed to the plasticizing effect of the bulky perfluoroacrylate pendant groups which increase the free volume for polymer chains. This result is also supported by the lower  $T_g$  of SP2 copolymer than SP1, which has more mol % PFA monomer, and also consistent with previous other studies with the perfluorinated polymethacrylate copolymers [34, 36]. All of the copolymers were detected to be rather soluble in THF as expected (rather transparent polymerization media without precipitates was observed after the polymerization was over), and trichloroethylene, except the GP was partially dissolved in trichloroethylene by leaving solid traces, which belong to the portions of the copolymer with higher molecular weight chains.

## 3.2 Surface properties of the copolymer smooth films

As it was mentioned in section 1.2, first of all, the copolymers should be sufficiently hydrophobic so that the physical condition of the surface would be in favor of air trapping if the surface roughness requirements are met further. Therefore, it is important to analyze the inherent hydrophobicity<sup>1</sup> of the copolymer surfaces, which can be performed by contact angle measurements on the smooth copolymer films. Thus, several copolymer films were prepared through different processes and roughness analysis of these films were made which would allow choosing the one whose roughness was low enough so that the surface could be assumed as smooth and contact angle analysis would not be affected from the roughness. Then by performing surface energy and water contact angle analysis of the surfaces, we would be able to decide whether the copolymers were hydrophobic enough to be employed in the generation of superhydrophobic surfaces by electrospinning.

### 3.2.1 Roughness analysis

Table 3.2 summarizes the surface topographic data of the copolymer films determined by AFM analysis. Although solution casting by TCE did not affect the final topographic properties of the MP copolymer film considerably when compared with solution casting by THF, the average ( $R_a$ ) and root mean square ( $R_q$ ) roughness values were rather low for the cast films of the SP1 and SP2 copolymer solutions in TCE. This should not be a result of the difference in the solubility of the copolymers in THF and TCE (THF was observed to be a better solvent since the dissolving rate of the copolymers in TCE was lower) but is attributed to the difference in the solvent evaporation rates of the films since THF is more volatile than TCE. Thus, TCE solutions were preferable for more smooth films and they were chosen for further improvement of the film smoothness by changing the coating method. However, for GP copolymer, THF was used as the solvent for each process since it was soluble in TCE. The influence of coating method on the final topography of the films was remarkable.

---

<sup>1</sup> Here the term inherent hydrophobicity refers to the hydrophobic properties of the copolymer surfaces resulting solely from the chemical groups at the outermost layer of the surface.

When compared with the solution cast films, the dip coated films were in general rather smooth, and smoother in a large extent than the solution cast films of the MP. This is mainly due to the thinner layer of solution during evaporation after dip coating that is known to have remarkable effect on the final physical properties of the polymer surfaces prepared from solutions [52]. Figure 3.1 represents the AFM images of the copolymer solution cast and dip coated films produced from TCE solutions. For the solution cast SP2 film, the surface was regularly covered by inverted-cone-like protrusions about 1-1.5  $\mu\text{m}$  in base diameter and 15 nm in height. For the dip coated films, there were holes about 200 nm in diameter on the MP and GP film surfaces. All of these structures probably occurred during the drying of the solutions, however this point is not directly within the scope of this study, but their possible effects on contact angle analysis will be discussed later in detail.

**Table 3.2** Roughness parameters for the cast films<sup>a</sup>

surface	coating method	$R_a$ (nm)	$R_q$ (nm)	$\Sigma$ (%)	$\Phi$ ( $^\circ$ )
MP	$S_{\text{THF}}$	$45.3 \pm 3.5$	$57.8 \pm 5.0$	<1	$0.77 \pm 0.15$
	$S_{\text{TCE}}$	$47.6 \pm 4.4$	$59.8 \pm 6.5$	<1	$0.80 \pm 0.16$
	$D_{\text{TCE}}$	$6.6 \pm 1.0$	$8.4 \pm 1.3$	<1	$0.15 \pm 0.02$
GP	$S_{\text{THF}}$	$29.9 \pm 6.5$	$39.9 \pm 10.2$	<1	$0.55 \pm 0.20$
	$S_{\text{TCE}}$	-	-	-	-
	$D_{\text{THF}}$	$2.1 \pm 0.9$	$3.7 \pm 1.8$	<1	$0.06 \pm 0.03$
SP1	$S_{\text{THF}}$	$6.1 \pm 0.8$	$13.5 \pm 1.5$	<1	$0.19 \pm 0.09$
	$S_{\text{TCE}}$	$1.6 \pm 0.3$	$3.6 \pm 0.4$	<1	$0.04 \pm 0.00$
	$D_{\text{TCE}}$	$0.34 \pm 0.0$	$0.7 \pm 0.2$	<1	$0.04 \pm 0.00$
SP2	$S_{\text{THF}}$	$14.0 \pm 1.2$	$20.7 \pm 2.1$	<1	$0.34 \pm 0.12$
	$S_{\text{TCE}}$	$5.8 \pm 0.0$	$8.0 \pm 0.3$	<1	$0.16 \pm 0.05$
	$D_{\text{TCE}}$	$0.6 \pm 0.0$	$1.2 \pm 0.4$	<1	$0.04 \pm 0.01$

<sup>a</sup>  $R_a$ ,  $R_q$ ,  $\sigma$  and  $\Phi$  are the number average roughness, the root mean square roughness, the ratio of actual to projected area and the average asperity rise angles, respectively, determined by AFM scans.  $S_{\text{THF}}$  and  $S_{\text{TCE}}$  refer to solution casting with tetrahydrofuran and trichloroethylene solutions, respectively.  $D_{\text{TCE}}$  refers to dip coating with trichloroethylene solution.

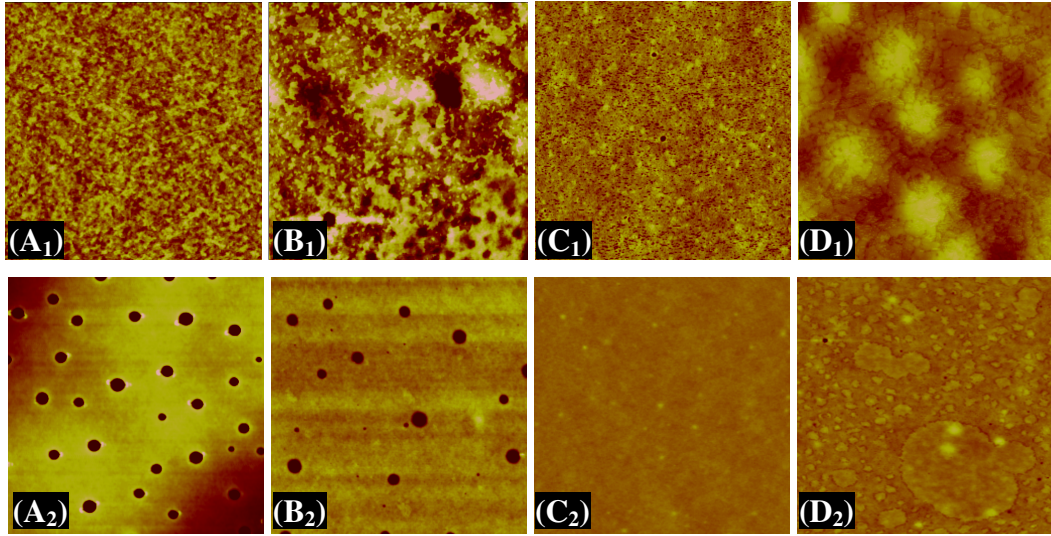


**Figure 3.1** AFM images ( $5 \times 5 \mu\text{m}^2$ ) of the copolymer films A) MP, B) GP, C) SP1 and D) SP2. Subscript 1 refers to solution casting and 2 refers to dip coating. Vertical scales are 10 nm for A<sub>1</sub>, B<sub>1</sub> and C<sub>1</sub>; 40 nm for D<sub>1</sub> and 30 nm for A<sub>2</sub>, B<sub>2</sub>, C<sub>2</sub> and D<sub>2</sub>

It was previously shown that  $R_a$  values below 100 nm generally does not effect contact angle analysis [2, 8, 53]. Among the dip coated films, the highest observed  $R_a$  value was  $6.6 \pm 1$  nm, which was the roughness of the MP dip coated film. Thus, the effect of roughness on the contact angle analysis would be insignificant. On the other hand, asperity rise angles ( $\Phi$ ) of the surfaces may be considered as the best parameter for gauging the influence of roughness on dynamic contact angles [8, 54, 55]. It was proposed that hysteresis due solely to roughness,  $\Delta\theta_{rnf}$ , depends on the asperity rise angles as [56]:

$$\Delta\theta_{rnf} = 2\Phi \quad (7)$$

It was experimentally shown that this equation can hold for randomly rough surfaces [55] so it can be effectively applied for the dip coated films. The highest observed  $\Phi$  on the films was 0.15, again on MP films, and Equation 7 predicts a  $0.3^\circ$  hysteresis that would be originating from the asperity rise slopes, therefore, this effect can also be neglected. In summary, all of the dip coated surfaces can be taken as ‘smooth’ and contact angle analysis and subsequent surface free energy calculations would not be affected by roughness. However, we chose the dip coated copolymer films for the contact angle analysis since they have the smoothest surface topography.

### 3.2.2 Surface free energy of the copolymer surfaces

**Table 3.3** Water, ethylene glycol and n-hexadecane advancing contact angles of the dip coated films and surface free energies

surface	$\theta_{\text{water}}$ ( $^{\circ}$ )	$\theta_{\text{ethylene-glycol}}$ ( $^{\circ}$ )	$\theta_{\text{n-hexadecane}}$ ( $^{\circ}$ )	$\gamma_{\text{sv}}^{\text{p}}$ (mN/m)	$\gamma_{\text{sv}}^{\text{d}}$ (mN/m)	$\gamma_{\text{sv}}$ (mN/m)
MP	114.4 $\pm$ 1.4	91.5 $\pm$ 1.2	57.3 $\pm$ 1.5	0.36 $\pm$ 0.03	15.53 $\pm$ 0.19	15.89 $\pm$ 0.22
GP	99.2 $\pm$ 0.8	81.8 $\pm$ 0.8	53.4 $\pm$ 0.8	2.39 $\pm$ 0.04	16.37 $\pm$ 0.11	18.76 $\pm$ 0.15
SP1	110.5 $\pm$ 0.4	89.7 $\pm$ 1.0	50.2 $\pm$ 0.8	0.25 $\pm$ 0.01	17.50 $\pm$ 0.11	17.76 $\pm$ 0.17
SP2	118.5 $\pm$ 0.5	95.4 $\pm$ 1.2	69.5 $\pm$ 0.9	0.12 $\pm$ 0.01	12.79 $\pm$ 0.11	12.91 $\pm$ 0.12

All of the surface free energies were relatively low and lower than that of PTFE which is 22 mN/m [44]. Although the PFA molar ratios in the copolymers were relatively low, their surface energies were much lower than those of the homopolymers of MMA, GMA and styrene, which are all above 30 mN/m. These results show that the perfluoroalkyl group exhibits vital function for decreasing the surface energy by arranging at the outermost layer. The long fluorinated chain itself and the CF<sub>3</sub> end group of PFA, which has the lowest surface energy, plays a major role for decreasing the surface energy lower than PTFE, which is solely composed of -CF<sub>2</sub>- groups. If a comparison is made between the surface energies of MP and SP1 films, one may be surprised that MP copolymer, although having polar segments from MMA and having lower PFA molar amount, has lower surface energy than the SP1 copolymer. However, this point can be explained by the combination of Equation 5 and 6. First of all, it is clear from Equation 5 that there is surface excess of PFA groups on all of the copolymer surfaces since PFA has the lowest surface energy in comparison with the other corresponding monomers. However, if we assume that we start to add the PFA monomer to the polymer chain by starting from pure poly(methyl methacrylate) (PMMA) and polystyrene (PS), the same amount of PFA addition would decrease the surface energies of these homopolymers differently. For instance, supposing that at a moment there are same percentage of PFA coverage,  $\Phi_{\text{P}}$ , on the surfaces of MP and SP1, then Equation 6 predicts that the surface energies will instantaneously equal to  $[\gamma_{\text{PFA}} \Phi_{\text{P}} + \gamma_{\text{MMA}} (1 - \Phi_{\text{PFA}})]$  for MP and  $[\gamma_{\text{PFA}} \Phi_{\text{P}} + \gamma_{\text{styrene}} (1 - \Phi_{\text{P}})]$  for SP. In addition, since the percent coverages of the PFA are equal, subsequently the increase in the

concentration of the PFA on the corresponding surfaces will be the same and the surface excess of PFA groups should depend only to the  $-\Delta\gamma$  since the other components of Equation 5 would be same (and become a positive constant) for two surfaces. Also, it can be supposed that the surface energies of PMMA and PS are equal to  $\gamma_{\text{MMA}}$  and  $\gamma_{\text{styrene}}$ , respectively. Then  $-\Delta\gamma$ , which can be assumed as  $-\Delta\gamma$ , will be equal to  $\Phi_{\text{P}}(\gamma_{\text{MMA}} - \gamma_{\text{PFA}})$  for MP and  $\Phi_{\text{P}}(\gamma_{\text{styrene}} - \gamma_{\text{PFA}})$  surfaces, respectively. And finally since  $\gamma_{\text{MMA}} > \gamma_{\text{styrene}}$  then there would be more excess of PFA for MP than for SP1. A general interpretation of this inference would be that the higher the surface energy of the starting material, the more the surface excess of PFA groups on the surface corresponding to the same amount of PFA addition.

When SP1 and SP2 copolymer surfaces are compared, it can be noticed that increasing the molar percent of the fluorinated monomer results further decrease in the surface energy but not to a large extent. This can again be explained by the inference made above. By starting with PS, which has a surface energy about 33 mN/m, when we add 6.8 mol % PFA to the chain, we synthesize the SP1 copolymer and the surface energy decreases by 15.25 mN/m to 17.76 mN/m. However, the SP2 copolymer can be assumed to be formed by a further addition of 6.2 mol % PFA to the SP1 copolymer that results a decrease of about 4.8 mN/m from 17.76 mN/m to 12.9 mN/m. These results are consistent with the inference made above: If PS is considered as the starting material for SP1, and SP1 as the starting material of SP2, consequently adding similar amounts of PFA to these starting materials results higher corresponding excess of PFA groups on the surface from PS to SP1 than from SP1 to SP2. A general interpretation of this event would be that the rate of decrease in the surface energy decreases with the increasing molar percent of the fluorinated monomer in the copolymer chain. Thus, for an experiment of step by step PFA addition to the copolymer chain, the resultant surface energy would be a decreasing and concave-up function of the mol % of PFA in the copolymer, which also indicates that the surface energy goes to the theoretical low limit by approaching to an asymptote rather than by a sharp decrease [34].

### 3.2.3 Dynamic contact angle analysis of the smooth copolymer films

Contact angle hysteresis is a direct measurement of a liquid's resistance to move on a surface. High hysteresis values cause pinned drops. As discussed in section 1.2, surfaces can still show measurable hysteresis values due to the adhesive bond between the solid surface and the liquid in the absence of imperfections such as roughness and chemical heterogeneities. Table 3.4 summarizes the dynamic contact angle analysis of water on the dip coated copolymer surfaces.

**Table 3.4** Dynamic contact angle analysis of the dip coated films

Surface	$\theta_a$ (°)	$\theta_r$ (°)	$\Delta\theta$ (°)
MP	114.4 ± 1.4	78.1 ± 1.0	36.3
GP	99.2 ± 0.8	58.0 ± 1.5	41.2
SP1	110.5 ± 0.4	92.1 ± 1.6	18.4
SP2	118.5 ± 0.5	98.1 ± 0.8	20.4

All of the surfaces exhibit notable hysteresis values. As we discussed in section 3.2.1 the analysis were not affected by the surface roughness and they were the results of the surface chemical properties solely. It is also worth noting that, dynamic contact angle analysis on the more rough, solution cast films of the copolymers showed very similar results with the dip coated films. This also indicates that effect of roughness is completely unimportant.

Other possible origin of hysteresis may be chemical heterogeneity but AFM phase images indicated that there is no macro phase separation on the films. In summary, it can be concluded that the primary reason for hysteresis was the molecular interaction between the solid surface and liquid, which may be due to the spontaneous rearrangement of polar or less hydrophobic groups to the surface when in contact with the liquid. Although this event may affect the receding angles dramatically by pinning the contact line, it was reported that it is not important for advancing contact angles [44]. Yet, this point is still unclear since the reasons of this behavior have remained less investigated throughout the hydrophobicity literature.

For deciding whether the copolymers were sufficiently hydrophobic or not, we refer to a study performed with polystyrene for the successful production of superhydrophobic surfaces by electrospinning [19]. Advancing contact angles on all of our copolymer smooth surfaces were greater than that on polystyrene, which is slightly higher than  $90^\circ$ , thus they had the potential to be employed in the production of superhydrophobic surfaces by electrospinning.

#### **3.2.4 Reorientation of polar groups to the surface due to water exposure**

Although section 3.2.3 concluded that the copolymers passed the test for the hydrophobicity requirement of electrospun superhydrophobic surfaces, a final investigation for the copolymer smooth films was proposed regarding the reorientation of polar groups to the surface due to water exposure. For this purpose, the copolymer smooth films were put under water and time dependent dynamic contact angle analysis were proposed to be performed in order to make a correlation and comparison for the change in the hydrophobic properties with the under-water treated electrospun copolymer surfaces discussed in section 3.3.3.

There are several reports monitoring the surface re-organization of amphiphilic copolymers due to water exposure via contact angle analysis [38, 42, 57]. Upon exposure to water, the higher surface energy groups started to orient to the solid-water interface. Accordingly, both the advancing and receding contact angles decreased. The preliminary experiments with our copolymer smooth films showed that all of our copolymers, particularly the amphiphilic ones (GP and MP), went under surface reorganization due to under-water treatment and both the advancing and receding contact angles decreased at the same time. However, the mechanical integrity of the films became corrupted with time within the water treatment which can affect the accuracy of the measurements. AFM results of the long interval water exposed films showed that after water exposure, particularly the surface roughness of the MP and GP surfaces increases remarkably to a level that can influence the contact angle analysis. For these reasons, the experiments were not carried on. Although time dependent contact angle data due to water exposure of smooth surfaces would be very helpful to

explain the physical condition of the water-treated rough surfaces described in section 3.3.3, we could anyway proposed several methods for this purpose that are discussed in the same section in detail.

### **3.3 Surface properties of the rough copolymer surfaces**

#### **3.3.1 Electrospinning of the copolymers**

In the section 3.2 it was shown that with their hydrophobicity, low surface energy and high solubility in common organic solvents, the copolymers were very appropriate for further processing with electrospinning. Previously, it was shown that electrospinning is a versatile method for producing tunable superhydrophobic surfaces [18, 21, 22]. It was experimentally [18, 21, 22] and theoretically [24] shown that advancing contact angles increase and sliding angles decrease by decreasing the solution concentration thus increasing the bead density in the electrospinning process. Similarly, electrospinning of 3 wt % concentration of the copolymers at 10 kV applied voltage resulted nearly fiber-free beads; however, in contrast to the acrylonitrile based copolymers electrospun solely in DMF in reference 18, these copolymers required nanofibers in order to interconnect the beads together and prevent the separation of microparticles from the surface by sticking onto the surface of water drops. Thus, we decided to keep the electrospinning solution concentration sufficiently low to get the most beaded surfaces but high enough to ensure their interconnection with small amount of nanometric fibers. SEM images of the electrospun surfaces are shown in Figure 3.2.

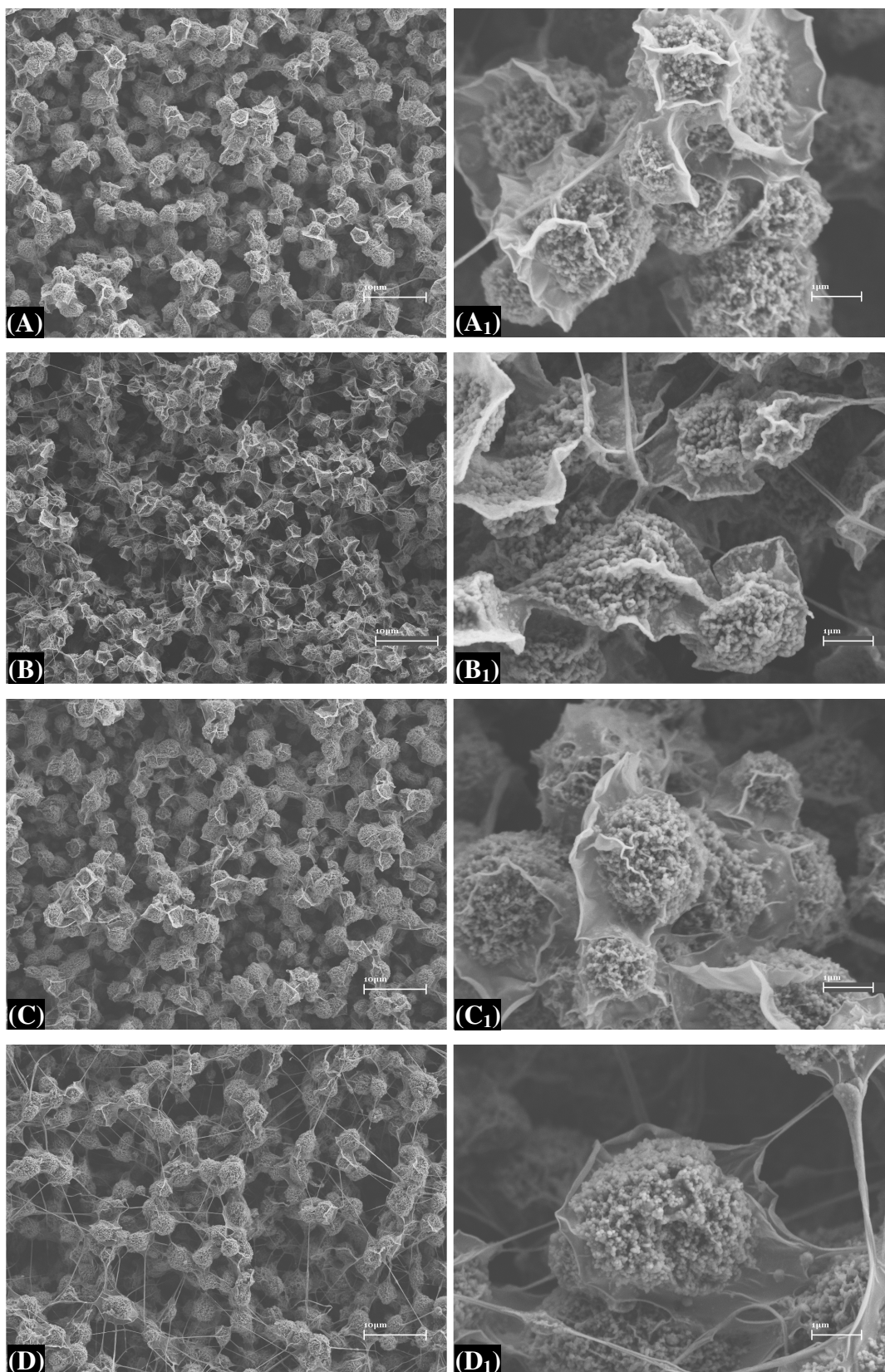


**Figure 3.2** Typical SEM images of the electrospun copolymer films A) MP, B) GP, C) SP1 and D) SP2. Subscript 1 represents the same surfaces at higher magnification. Scale bars correspond to 10 and 1  $\mu\text{m}$  for the left and right images, respectively.

SEM analysis showed that the nanofiber concentration of the SP2 films were the most although it was difficult to differentiate the fiber amount between the surfaces of other copolymers. The relatively higher fiber amount of the SP2 films was attributed to the higher viscosity of the solution due to the higher molecular weight of the copolymer.

### **3.3.2 Dynamic contact angle analysis of the electrospun copolymer surfaces**

Table 3.5 shows the advancing and receding contact angle analysis of the electrospun surfaces shown in Figure 3.2. All of the surfaces showed contact angle hysteresis smaller than 7 degrees and consequent low sliding angles. Thus all of the surfaces were both superhydrophobic and ultrahydrophobic. As discussed in detail in section 1.3, while a drop moves on an ultrahydrophobic surface, it jumps from one metastable state to another by overcoming the energy barriers determined by the shape, length, continuity and amount of contact of the three phase contact line. The high water repellence of these electrospun surfaces is attributed to the relatively low surface energy of the copolymers that would support the formation of the composite surface, and to the very well separation of the micro-beads in three dimensions, on which a very discontinuous and lengthy three phase contact line is supposed to form. In addition, Gao and McCarthy [9, 58] very recently explained that the nanometer scale physical formations on micron scale roughness, such as the nanometer wax crystals on the Lotus leaves, are crucial for the easy receding of the contact lines. If the individual beads in Figure 3.2 are examined in detail, it would be noticed that the bead surfaces were covered with smaller beads in the range of 40 to 70 nm, which were formed due to very rapid evaporation of the solvent during electrospinning. In addition to the discontinuity of the three phase contact lines on the electrospun surfaces, these nano-beads function to increase the receding angles to a level that also contributes significantly for the observed low hysteresis values.

**Table 3.5** Dynamic contact angle analysis of the as produced electrospun films

Surface	$\theta_a$ (°)	$\theta_r$ (°)	$\Delta\theta$ (°)	Sliding angle (°)
MP	162.4 ± 0.9	156.0 ± 1.2	6.4	5.6 ± 0.4
GP	162.9 ± 0.6	158.8 ± 1.0	4.1	3.6 ± 0.2
SP1	160.1 ± 1.2	155.9 ± 1.5	4.2	3.8 ± 0.4
SP2	160.4 ± 0.8	155.2 ± 0.5	5.2	4.6 ± 0.4

At a first sight, it may be surprising that the lowest surface energy copolymer, SP2, resulted in higher hysteresis and sliding angle values than the SP1 and GP electrospun surface which are of relatively higher surface energy. A relation between the smooth surface chemistry and rough surface hydrophobicity may be constructed with superhydrophobic and ultrahydrophobic surfaces of well defined topology [10, 11, 59-61]. However, such a direct correlation for electrospun surfaces, which are randomly rough in 3D, would be misleading since neither the exact values of  $f_1$  in the Cassie-Baxter equation can be evaluated nor the exact physical structure of the three phase contact line is analytically possible to monitor. However the events occurring at the three phase contact line during advancing and receding is of crucial concern where the slight deviations in the interfacial energy of the polymers itself is largely dominated [9].

### 3.3.3 Effect of surface reorientation due to water exposure on electrospun films

Previous section showed that the copolymers can be used for the production of superhydrophobic and ultrahydrophobic surfaces effectively. However, as it was stated earlier in section 3.2.4, the copolymer surfaces can become slightly less hydrophobic for the SP1 and SP2 films, and in a large extent for MP and GP films due to continuous contact with water. For the electrospun surfaces, this event would also affect the water repellence of the surfaces. However, since the surface reorganization due to water exposure is a contact based incidence, in other words, since it occurs only among the solid-liquid interface, the effect might be different from the smooth films because of the composite interface structure of the electrospun surfaces where a mixture of solid-liquid

and solid-vapor interfaces existed. In order to examine the stability of the electrospun copolymer surfaces against water contact, we placed electrospun samples under water and investigated their response to water exposure via contact and sliding angle analysis. Table 3.6 summarizes the contact angle analysis after 11 days of water treatment and Figure 3.3 shows the corresponding time dependent sliding angle values.

**Table 3.6** Dynamic contact angle analysis of the electrospun films after 11 days of water exposure

Surface	$\theta_a$ (°)	$\theta_r$ (°)	$\Delta\theta$ (°)	Sliding angle (°)
MP	$152.8 \pm 2.5$	$90.7 \pm 5.1$	62.1	no sliding
GP	$156.1 \pm 2.6$	$116.2 \pm 3.9$	39.9	$50.0 \pm 4.24$
SP1	$160.0 \pm 0.6$	$152.4 \pm 1.48$	07.6	$08.2 \pm 1.38$
SP2	$159.5 \pm 0.8$	$151.2 \pm 1.67$	08.3	$12.2 \pm 1.25$

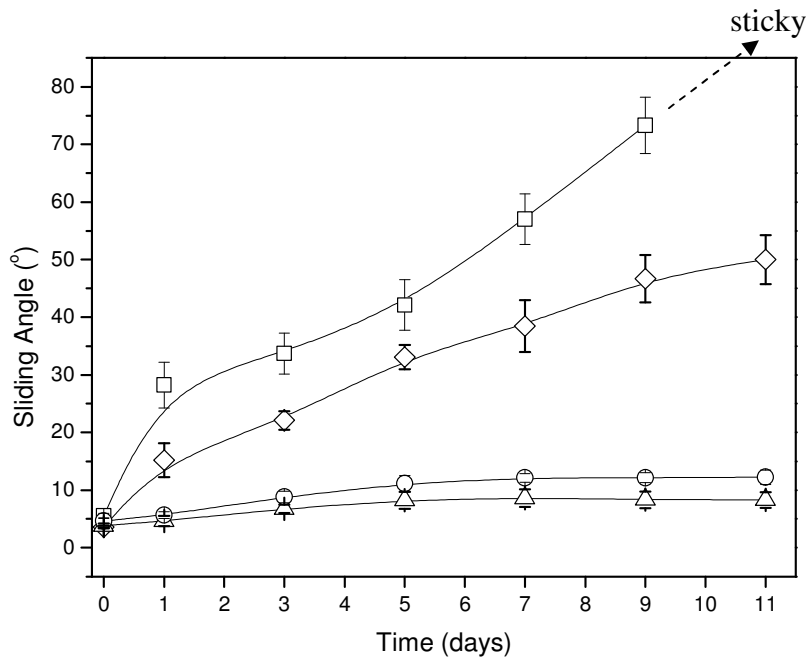


**Figure 3.3** Sliding angles vs exposure time to water for the copolymer electrospun films MP (□), GM (◇), SP1 (△) and SP2 (○)

Within 11 days of water exposure, hysteresis and sliding angles of the surfaces increased for all of the surfaces. However, the difference was very obvious for the amphiphilic GM and MP copolymers where the values changed slightly for the SP1 and SP2 copolymers. Although the surface topology remained unchanged during water exposure, which was ensured by SEM analysis after water treatment, the orientation of polar groups of the MP and GP copolymers to the solid-water interface greatly affected the surface energy after emersion to air and the apparent advancing angle,  $\theta^*$  decreased accordingly. Although all of the surfaces were still superhydrophobic ( $\theta^* > 150^\circ$ ), it was clear that water treatment affected ultrahydrophobicity greatly for GP and made the MP a sticky surface.

There may be several reasons for why the water treated electrospun MP surface became sticky:

1. It may be thought that for the MP and GP copolymers, since the interfacial energy increases due to reorientation of the polar groups to the outermost surface, the chemical requirement for being a composite surface (i.e. the surface should be hydrophobic enough to prevent the penetration of water into the cavities) was lost and the surface transformed into the Wenzel state by step by step wetting through the walls of the cavities into the deeps.
2. It may be claimed that the water treated MP surface may be in a metastable Cassie-Baxter state which are also characterized by sticky drops [49].
3. The reorientation may have occurred primarily on the top of the protrusions (but the surface energy of the interior surface of the cavities remained unchanged) so the composite structure was maintained whereas enhanced adhesive bonds between the discontinuous TPCL and the top of the protrusions prevented the disjoining of the TPCL during receding and the surface became sticky.

*Was the water treated electrospun MP surface in the Wenzel state?*

In order to answer this question, the difference between the physical states of the TPCL on a smooth, Wenzel and Cassie-Baxter surface should be understood well. Figure 3.4 shows the possible TPCLs in these three types of states:

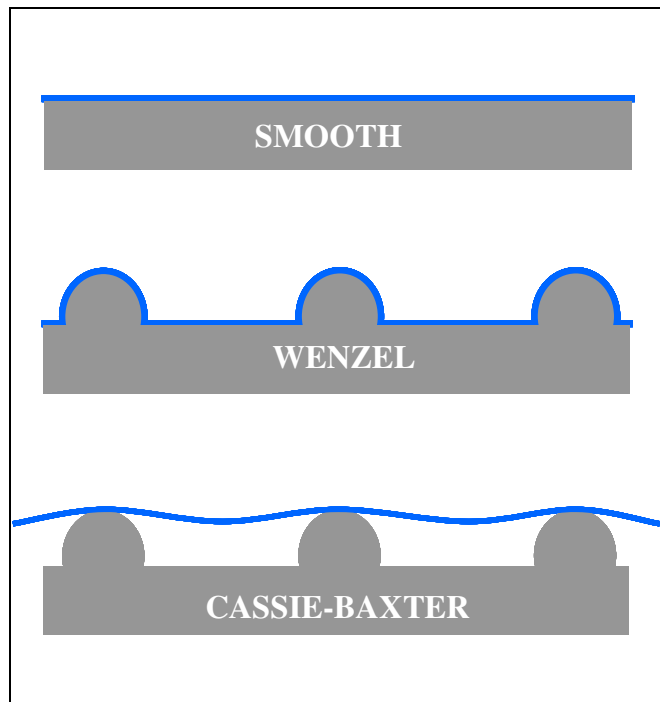


**Figure 3.4** Shapes of TPCLs in different states. Gray regions represent the solid surface. Blue lines represent the water molecules within the TPCL

If it is assumed that all the three surfaces in Figure 3.4 are of same surface energy material<sup>2</sup>, then it would be comprehensible that the amount of contact for the projected length of the TPCL for Wenzel is the highest and for Cassie-Baxter, the lowest. Thus the total adhesive bonds between the solid and liquid will be highest for the Wenzel state so there would be much energy barrier for the TPCL to disjoin from the surface. This energy barrier can be overcome by more bending of the drop at the receding side which microscopically increases the horizontal component of the liquid-vapor interface vector as it can be seen in the Figure 3.5 by decreasing the receding angle  $\theta_r$ .

---

<sup>2</sup> It is in fact impossible to observe both the Wenzel and Cassie-Baxter regimes (with a certain liquid) for a surface of same topography and same hydrophobicity. Either one should occur in reality. However, the states in the model should be considered as ‘what would happen if the surfaces were in the Wenzel state and in the Cassie-Baxter state’ when compared with the smooth surface.

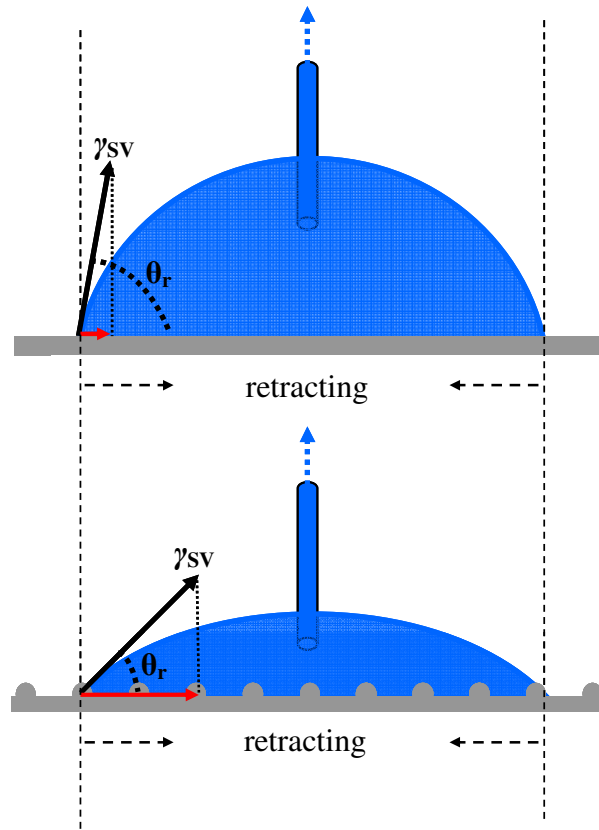


**Figure 3.5** Physical events that occur during receding of a water drop on a smooth (up) and Wenzel (down) surface

From these discussions we can conclude that receding angle for a liquid in Wenzel regime must be smaller than that on a smooth surface (of same surface energy) in all of the cases. In addition, as it was mentioned in section 3.2.4, the receding contact angles of the water treated smooth surfaces decrease due to reorientation of polar groups which results enhanced solid-water adhesive bonds so increases the activation barrier of the TPCL during retracting from the smooth surface. However, it should be noted that only for a Cassie-Baxter surface of discrete protrusions, on which a discontinuous TPCL can occur we can in general claim that the receding angle would be the highest. But if the topography of the composite surface is composed of continuous structures, then the receding angle may even be the lowest. In other words, depending on the physical state of the TPCL of a drop on a Cassie-Baxter state, the receding angle can take any value between 0 and 180°.

In summary, for a certain surface energy material which can undergo reorientation of polar groups to the surface when exposed to water, the relation of receding angles between different surface states is made by the inductions:

$$\begin{aligned}
 & \theta_r^{\text{wenzel}} < \theta_r^{\text{smooth}} \\
 \rightarrow & \theta_r^{\text{water-treated-wenzel}} < \theta_r^{\text{water-treated-smooth}} \\
 & \theta_r^{\text{water-treated-smooth}} < \theta_r^{\text{smooth}} \\
 \rightarrow & \theta_r^{\text{water-treated-wenzel}} < \theta_r^{\text{smooth}} \quad (\text{A})
 \end{aligned}$$

The summary of A is that if the water treated electrospun MP surface was in Wenzel state, then the receding angle would be much smaller than that on the untreated smooth surface, which was  $78.1^\circ$ . However, the receding angle on this surface was  $90.7^\circ$  (Table 3.6). Thus, it was certain that the surface was not in the Wenzel regime after water treatment.

*Was the water treated electrospun MP surface in a metastable Cassie-Baxter state?*

In order to answer this question, the physical conditions of metastable Cassie-Baxter state should be understood well. As it was stated several times before, transformation to a Cassie-Baxter state can only occur for a combined sufficient inherent hydrophobicity and roughness. Another interpretation of this statement is that the nature of the texture design of the surface determines an inherent hydrophobicity of the surface (smooth film contact angle of the solid) over which the transformation to the Cassie-Baxter state occurs. If this critical contact angle is denoted by  $\theta_c$ , and the inherent hydrophobicity of the surface is by  $\theta$ , then:

$$\begin{aligned}
 & \text{If } 90 < \theta < \theta_c, \text{ then Wenzel state must occur} \\
 & \text{If } \theta > \theta_c, \text{ then Cassie-Baxter state must occur}
 \end{aligned}$$

However, it has often been reported that the Cassie-Baxter regime can also be observed for  $\theta < \theta_c$ , which is termed as the metastable Cassie-Baxter state [49]. On the other hand, if a pressure is applied to the drop so that water is forced to penetrate into

the cavities, the surface cannot resist and transforms to Wenzel state irreversibly. A schematic representation of this phenomenon is shown in Figure 3.6.

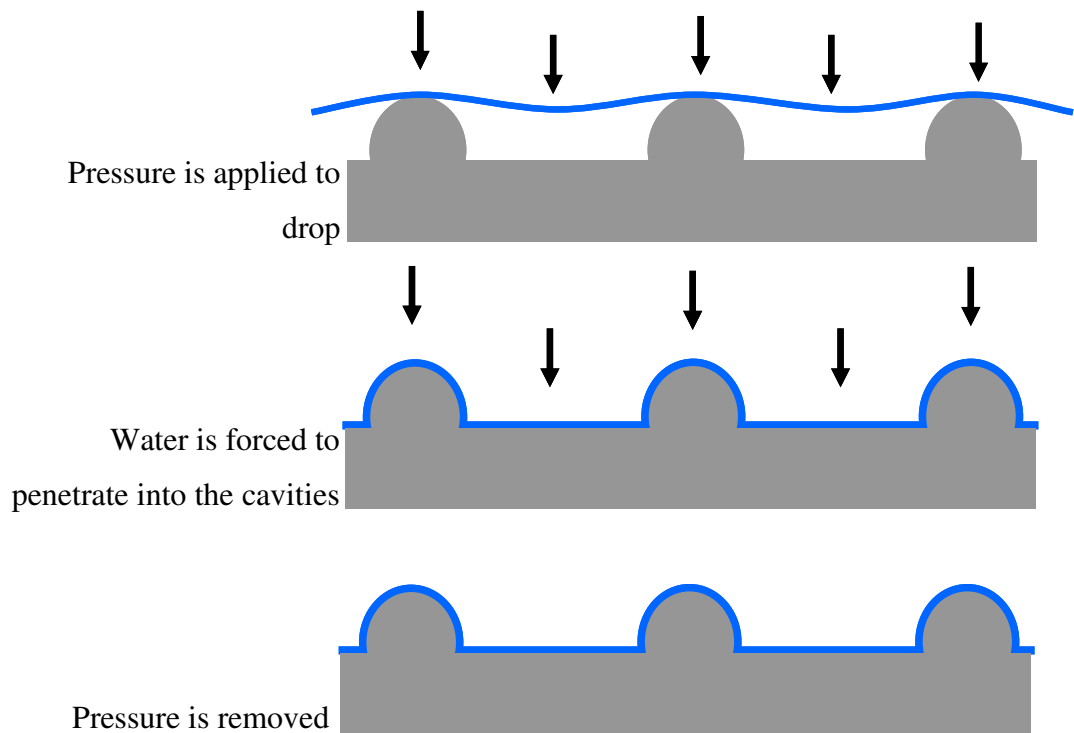


**Figure 3.6** The change in the TPCL when pressure is applied to a drop in a metastable Cassie-Baxter state. Gray regions represent the solid surface. Blue lines represent the water molecules within the TPCL

So, if the water treated electrospun MP surface was in a metastable Cassie-Baxter state, then a pressure application would transform it to the Wenzel state. Then, all of the discussions made under the previous question would apply to this pressed drop. In other words,

$$\theta_r^{\text{water-treated-pressed}} < \theta_r^{\text{smooth}}$$

For this, pressure was applied to a drop sitting on the treated electrospun MP surface from upwards with the help of another ultrahydrophobic surface for 10 minutes. After removing the pressure, we measured the receding angle and found out that it was however around  $88^\circ$ . Thus, it is also certain that the surface was not in a metastable Cassie-Baxter state.

*Was the drop on the treated electrospun MP surface pinned due to the enhanced adhesive bonds on the top of the protrusion?*

The discussions just made clearly show that the surface was still in the Cassie-Baxter regime. This brings out that the TPCL was still discontinuous and the amount of contact with the surface was still low. So the main reason for contact line pinning was solely due to the largely increased adhesive bonds where the TPCL and the solid surface contacted each other as it was schematically shown by the red regions in Figure 3.7. The reason for this partial reorganization of the surface was that when the sample was put under water, initially only the top of the protrusion, where the solid-liquid interface occurred, started to go under reorganization easily; however, this polarity change on the contacting regions could not continue along the perimeter of the contacting area towards the deeps of the cavity walls easily because of the high Laplace pressure enhanced by the high advancing contact angles [58]. Consequently, only the surface energy of the top of the protrusions decreased but the walls of the cavities maintained the hydrophobic character. Thus a pressure application to the drop, which can force water to penetrate into the cavities, did not change the composite structure of the surface.

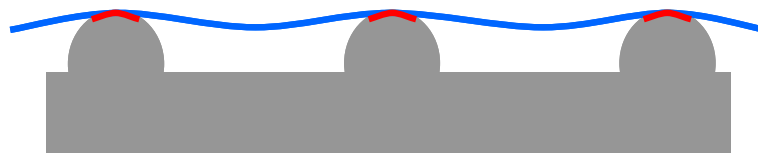


**Figure 3.7** The state of the TPCL on the water treated electrospun MP surface. Red lines show the regions went under reorganization due to water exposure

There are two significant result of this experiment: First, it was shown that adhesive strength between the solid and the TPCL is as important as the shape, length, continuity and amount of contact of the TPCL for determining the energy barriers to receding. This point had been dismissed in the water repellency literature. Second, Cassie-Baxter equation can only be used to formulate the advancing contact angles on the rough surfaces; they cannot be employed to rationalize the sliding behavior of the water drops on different surfaces. For instance, since the electrospun MP surface after water treatment preserved the composite structure, it still showed superhydrophobicity

(contact angle  $> 150^\circ$ ). However, receding contact angles are directly related with the TPCL which in fact determines the dynamic behavior of water on surfaces.

### 3.3.4 Improving the non-wetting of the reorganization-resistive surfaces

Results of the wettability tests on the electrospun surfaces before and after water treatment clearly showed that the electrospun SP1 and SP2 surfaces can maintain their water repellence against water exposure for long intervals. However, although they showed superior property in this term, they still had possible room for improving the ultrahydrophobic character further; in other words, the hysteresis could still be decreased. For this purpose, the SP2 copolymer was chosen for further improvement since it had higher PFA amount. There were several methods for this:

1. One possible method was increasing the hydrophobicity by adding more PFA to the polymer chain. Nevertheless, the SP2 copolymer had an advancing contact angle of about  $118^\circ$  and this was close to the upper limit for such polymer since the highest advancing contact angle on a smooth surface was reported to be  $122^\circ$  and that could be achieved only by regular arrangement of the  $\text{CF}_3$  groups [4]. Thus, this limit was not possible to reach by the methods used for the preparation of the polymers reported in section 2.2. Be that as it may, it would not make so much difference for the electrospun surfaces because although the SP2 copolymer had  $8^\circ$  higher smooth film contact angle than the SP1 copolymer, they had nearly the same water repellence properties in the electrospun form.
2. Improving the topography of the electrospun surface of SP2 copolymer in a fashion that would minimize the fiber amount and increase the bead density may have been useful.

For this purpose we prepared a 2 w % 1:1 THF:DMF solution of the SP2 copolymer and electrospun it with the same conditions as the 3 w % one but changed the applied voltage to 8 kV. As it can be compared from the SEM images in Figure 3.8 and Figure 3.9, this reduction in the concentration resulted in nearly fiber free beads and

allowed decreasing the sliding angle by  $1.8^\circ$  from  $4.6^\circ$  to  $2.8^\circ$ . The advancing/receding contact angles were  $158.5^\circ/156.3^\circ$ . It was clear that decreasing the concentration further had the possibility of more improved results but could also cause breaking the interconnection of the beads which would lead to the separation of microparticles from the surface by sticking onto the surface of water drops.

The influence of increasing applied voltage has been known to have strong effects on the morphologies of electrospun fibers but the same effect somehow still remains to be less investigated for the bead structures. Accordingly, this time the applied voltage was increased for the 2 w % SP2 copolymer solution. When it was electrospun at 11.5 kV, the beads came closer and their population increased further as it can be seen in Figure 3.10. However, by this process, we could decrease the sliding angle to  $0.9^\circ$ . The advancing/receding contact angles were  $160.1^\circ/158.9^\circ$ .

Gao and McCarthy [9, 58] recently explained the Lotus effect in terms of the influence of two length scales of topography on low hysteresis values. They showed that the hysteresis on a superhydrophobic surface can be decreased effectively without changing the chemical properties of the surface but introducing nanometer scale topography on the micron scale protrusions that would increase the receding contact angles locally (on the protrusions themselves) and so, would decrease the hysteresis. Inspired from this point it was decided to get rid of the nano films which existed between the beads (Figure 3.10). This could be achieved by increasing the voltage further to 15 kV. The result was remarkable; the surface was composed of joint beads and not only the surface of the beads but also every region on the surface was covered with nanometric roughness (Figure 3.11). This superior structure resulted in a zero hysteresis surface (advancing/receding was  $162.2^\circ/162.2^\circ$ ) on which a drop could not be immobilized for measuring the sliding angle which was very close to zero.

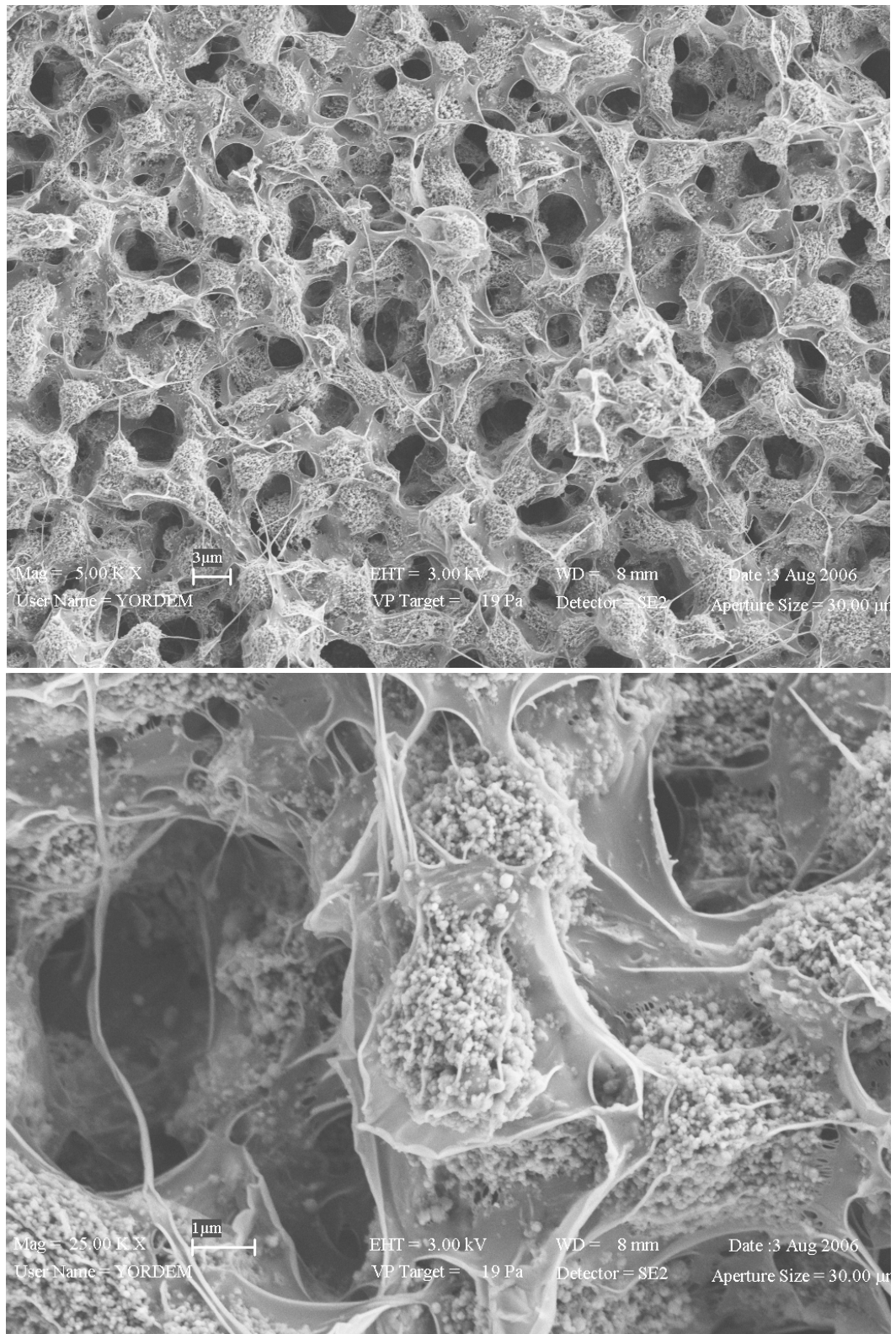


**Figure 3.8** Electrospun surfaces of the SP2 copolymer at 2 w % concentration and 8 kV applied voltage. Magnifications are 5000 and 25000 for upper and lower images, respectively

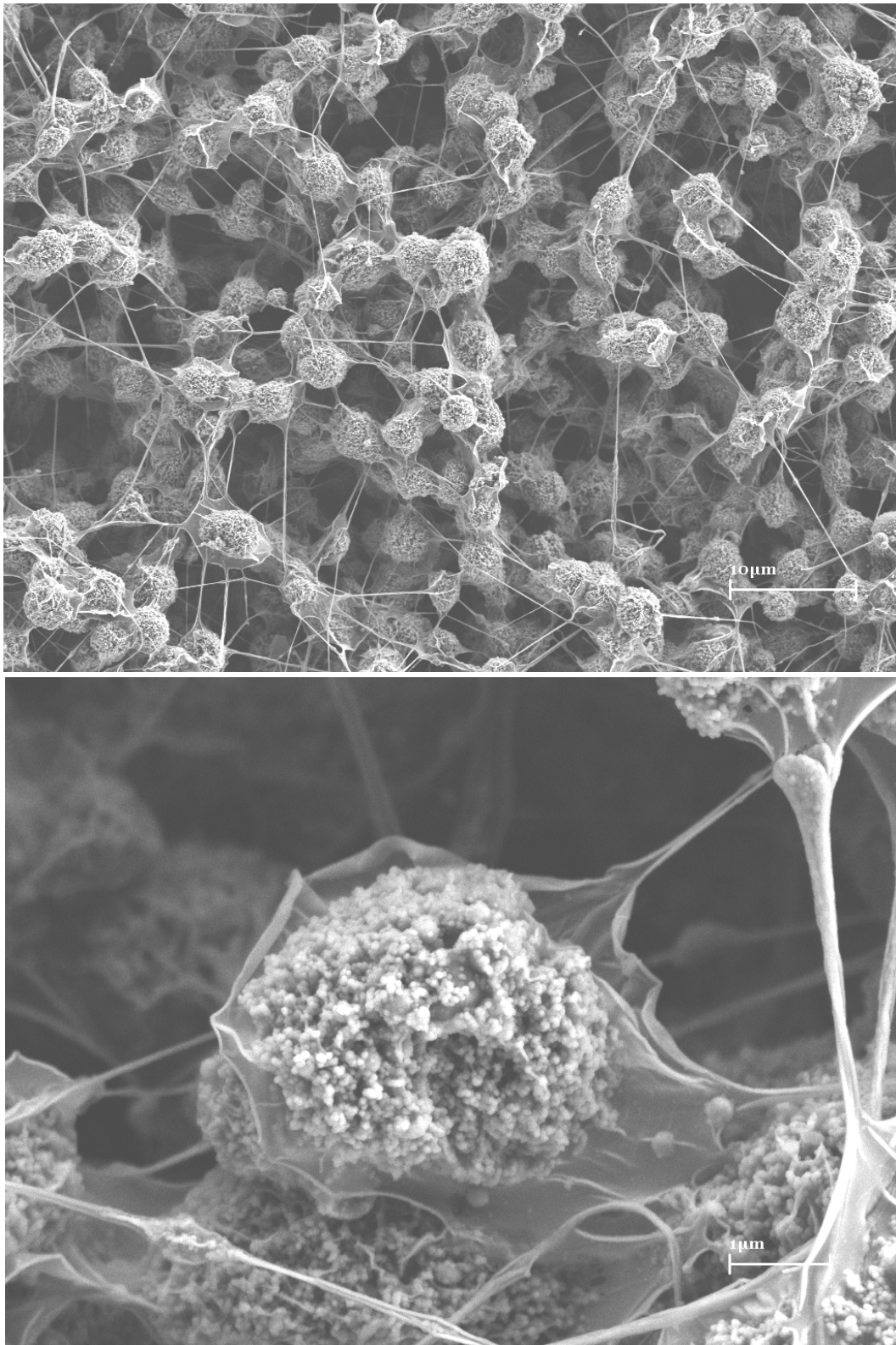


**Figure 3.9** Electrospun surfaces of the SP2 copolymer at 3 w % concentration and 8 kV applied voltage. Magnifications are 5000 and 40000 for upper and lower images, respectively. This image is the same as Figure 3.2-D but put for comparison.

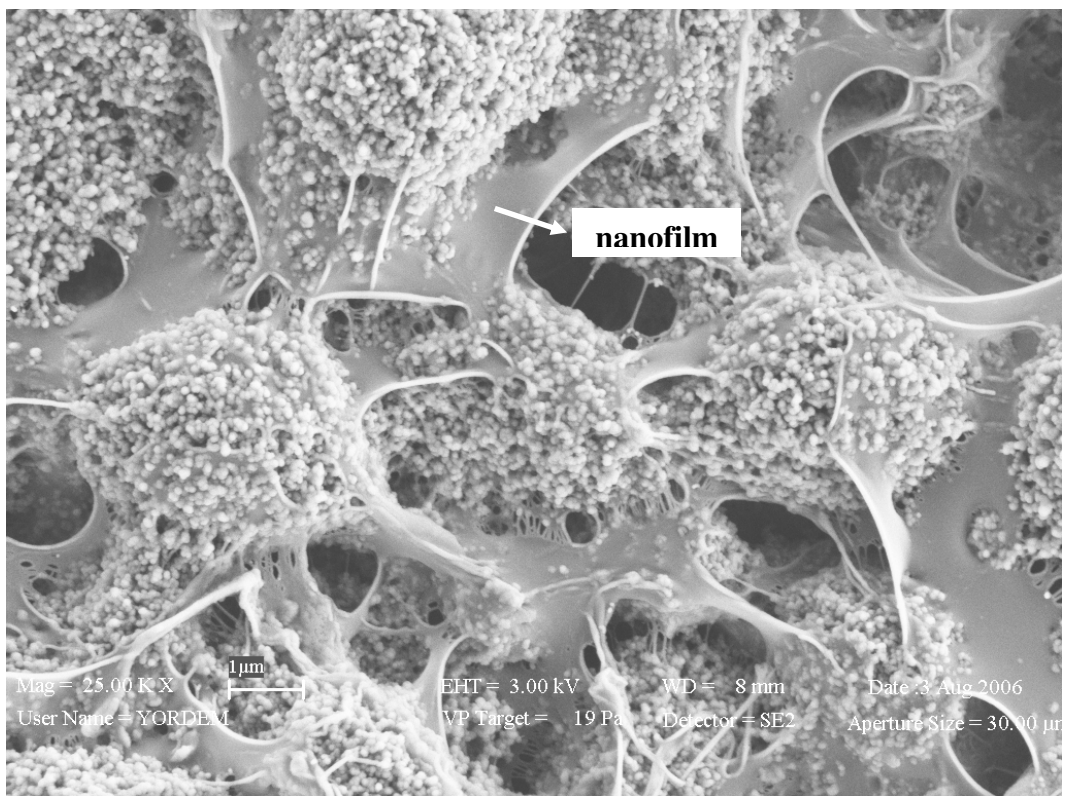
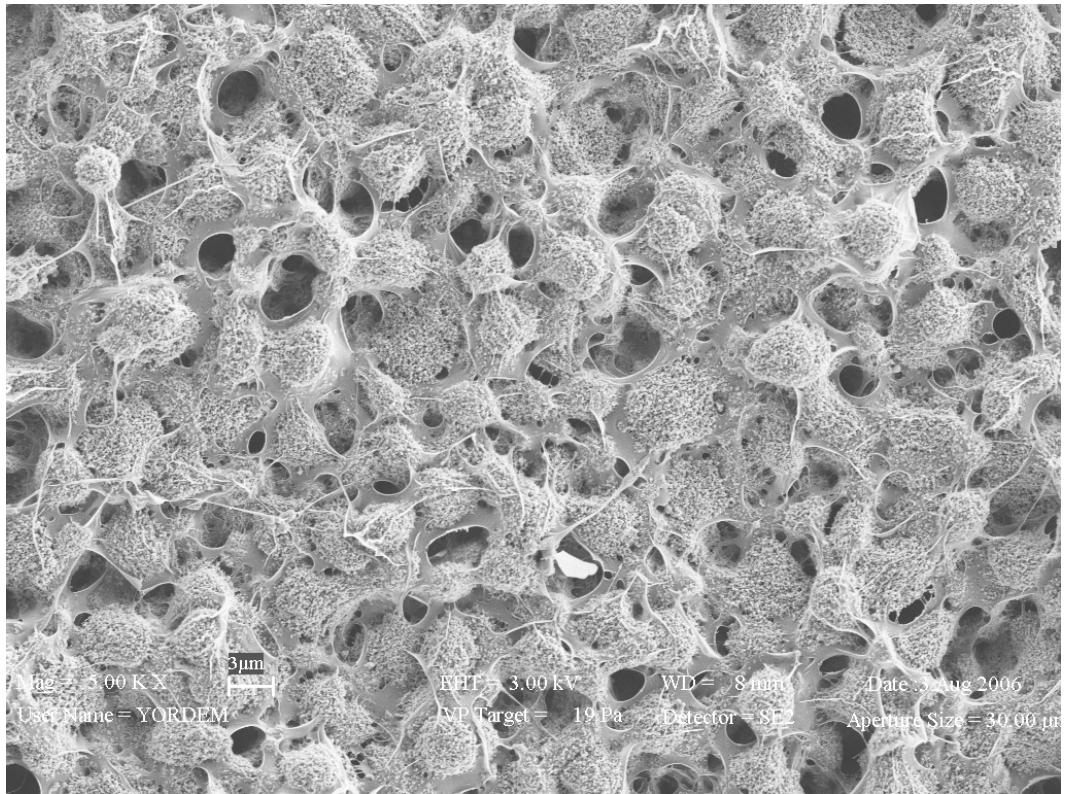


**Figure 3.10** Electrospun surfaces of the SP2 copolymer at 2 w % concentration and 11.5 kV applied voltage. Magnifications are 5000 and 25000 for upper and lower images, respectively

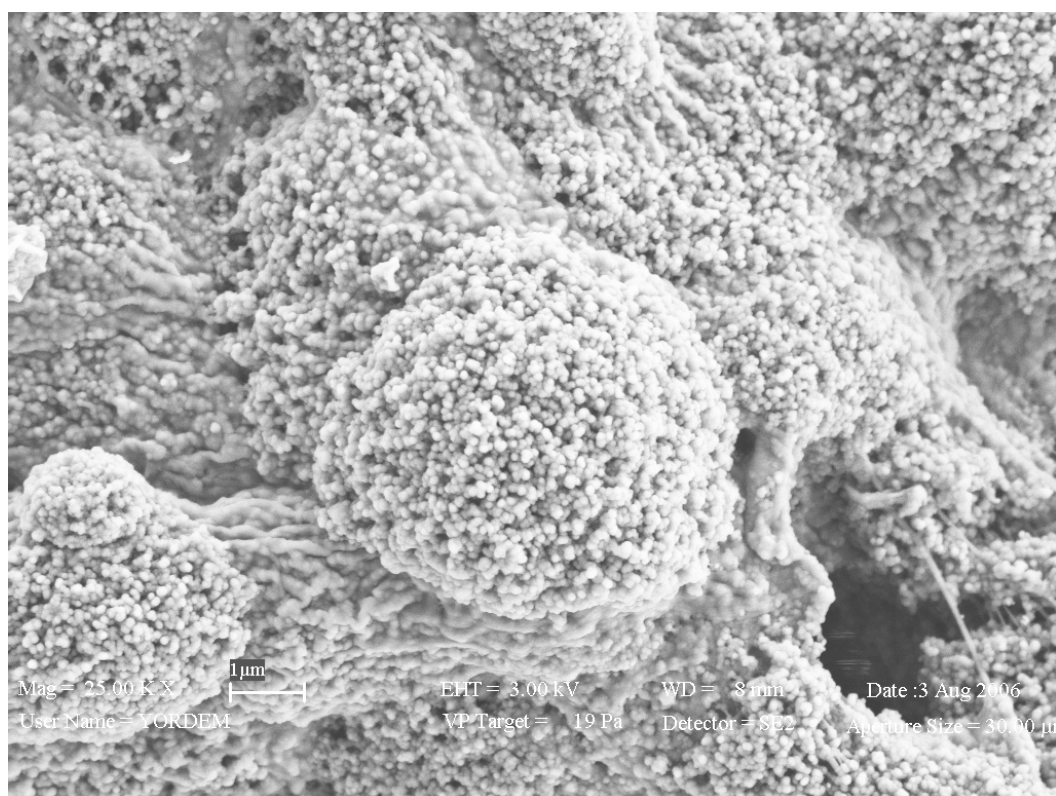
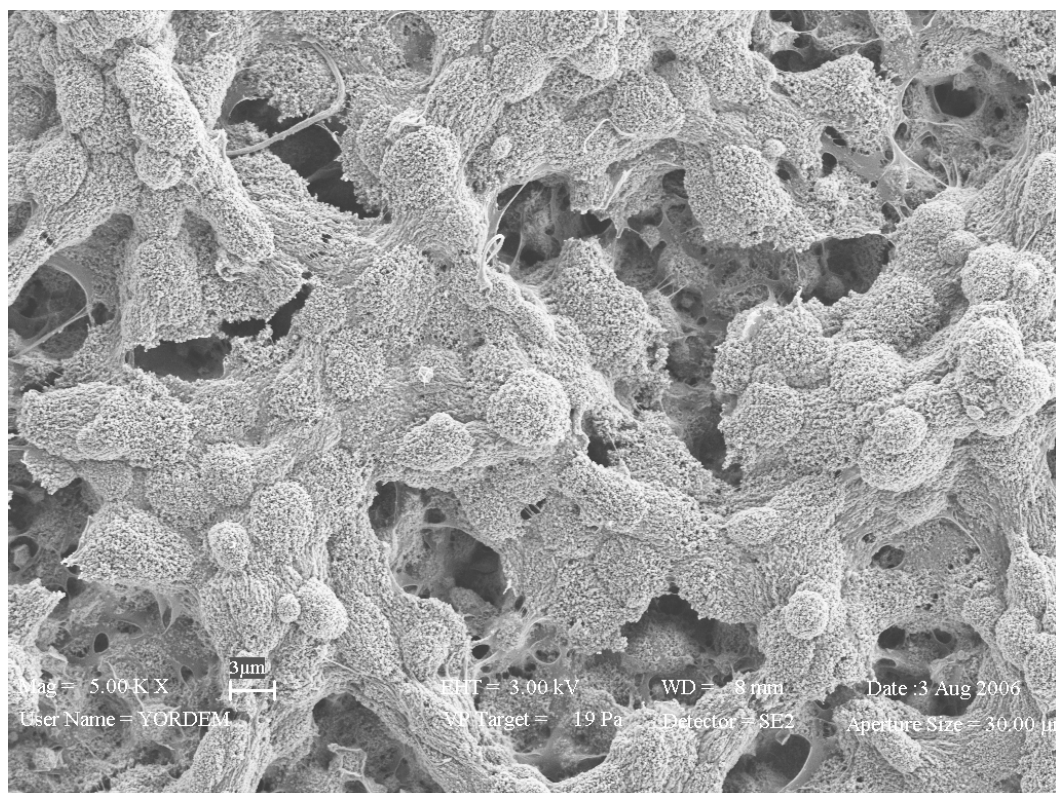


**Figure 3.11** Electrospun surfaces of the SP2 copolymer at 2 w % concentration and 15 kV applied voltage. Magnifications are 5000 and 25000 for upper and lower images, respectively

#### 4. CONCLUSION

This study showed that perfluoroacrylate copolymers can be effectively used for the production of ultrahydrophobic surfaces via electrospinning. Small amounts of perfluoroacrylate in the copolymers were sufficient to achieve low surface energy polymers due to arrangement of fluorinated groups at the outermost surface. It was also shown that amphiphilic copolymers can have lower surface energy than non-polar copolymers because of the higher excess of the fluorinated groups on the surface. When the roughness requirements were met by electrospinning of the copolymers, they could be easily transformed into ultrahydrophobic surfaces. However, the bulk monomer composition was crucial for the stability of the surfaces against water contact. After eleven days of water exposure, the ultrahydrophobicity of the amphiphilic copolymers was lost due to enhanced adhesive bonds between the solid surface and water that prevented the disjoining of the three phase contact line from the tops of the protrusions during receding. Thus, the strength of the adhesive bonds at the contacting regions with the solid surface was proven to be as significant as the other physical properties such as discontinuity, length and amount of contact of the three phase contact line. On the other hand, superhydrophobicity was preserved during water exposure since water could not penetrate into the cavities because of the high Laplace pressure, so the inner surfaces of the cavities preserved hydrophobic nature. Consequently, high advancing contact angles were maintained so the surfaces were still superhydrophobic.

The first part of the study showed the importance of the monomer selection in the stability of the ultrahydrophobic surfaces produced from perfluoroacrylate copolymers to long interval water contact. In the second part, it was shown that two level roughness was very significant for decreasing the contact angle hysteresis and achieving perfectly non-wetting surfaces. The formation of nanometer scale beads on the entire rough surface due to high applied voltage during electrospinning of low concentration

copolymer solutions resulted in a zero hysteresis ultrahydrophobic surface which was observed to have no physical attraction with water drops.

## REFERENCES

1. Shaw, D. J., *Introduction to Colloid and Surface Chemistry*. 4 ed. Elsevier Science, Burlington, 1992.
2. Kwok, D. Y. & Neumann, A. W. Contact angle measurement and contact angle interpretation. *Adv Colloid Interfac* **81**, 167 (1999).
3. Young, T. An Essay on the Cohesion of Fluids. *Philos Trans R Soc London* **95**, 65 (1805).
4. Nishino, T., Meguro, M., Nakamae, K., Matsushita, M. & Ueda, Y. The lowest surface free energy based on -CF<sub>3</sub> alignment. *Langmuir* **15**, 4321 (1999).
5. Chen, Y. L., Helm, C. A. & Israelachvili, J. N. Molecular mechanisms associated with adhesion and contact angle hysteresis of monolayer surfaces. *J Phys Chem* **95**, 10736 (1991).
6. Extrand, C. W. & Kumagai, Y. An experimental study of contact angle hysteresis. *J Colloid Interf Sci* **191**, 378 (1997).
7. Extrand, C. W. A thermodynamic model for contact angle hysteresis. *J Colloid Interf Sci* **207**, 11 (1998).
8. Extrand, C. W. Contact angles and their hysteresis as a measure of liquid-solid adhesion. *Langmuir* **20**, 4017 (2004).
9. Gao, L. C. & McCarthy, T. J. Contact angle hysteresis explained. *Langmuir* **22**, 6234 (2006).
10. Oner, D. & McCarthy, T. J. Ultrahydrophobic surfaces. Effects of topography length scales on wettability. *Langmuir* **16**, 7777 (2000).
11. Chen, W., Fadeev, A. Y., Hsieh, M. C., Oner, D., Youngblood, J. & McCarthy, T. J. Ultrahydrophobic and ultralyophobic surfaces: Some comments and examples. *Langmuir* **15**, 3395 (1999).
12. Youngblood, J. P. & McCarthy, T. J. Ultrahydrophobic polymer surfaces prepared by simultaneous ablation of polypropylene and sputtering of poly(tetrafluoroethylene) using radio frequency plasma. *Macromolecules* **32**, 6800 (1999).

13. Furmidge, C. G. L. Studies at phase interfaces. I. The sliding of liquid drops on solid surfaces and a theory for spray retention. *J Colloid Interf Sci* **17**, 309 (1962).
14. Wenzel, R. N. Resistance of solid surfaces to wetting by water. *Ind Eng Chem* **28**, 988 (1936).
15. Cassie, A. B. D. & Baxter, S. Wettability of porous surfaces. *Trans Faraday Soc* **3**, 16 (1944).
16. Dettre, R. H. & Johnson Jr., R. E. Contact angle, Wettability and Adhesion. *Adv Chem Ser* **43**, 112 (1964).
17. Barthlott, W. & Neinhuis, C. Purity of the sacred lotus, or escape from contamination in biological surfaces. *Planta* **202**, 1 (1997).
18. Acatay, K., Simsek, E., Ow-Yang, C. & Menciloglu, Y. Z. Tunable, superhydrophobically stable polymeric surfaces by electrospinning. *Angew Chem Int Edit* **43**, 5210 (2004).
19. Jiang, L., Zhao, Y. & Zhai, J. A lotus-leaf-like superhydrophobic surface: A porous microsphere/nanofiber composite film prepared by electrohydrodynamics. *Angew Chem Int Edit* **43**, 4338 (2004).
20. Agarwal, S., Horst, S. & Bognitzki, M. Electrospinning of fluorinated polymers: Formation of superhydrophobic surfaces. *Macromol Mater Eng* **291**, 592 (2006).
21. Simsek, E., Yordem, O. S., Menciloglu, Y. Z. & Papila, M. Optimization of superhydrophobic surfaces generated by electrospinning. *Polym Mater Sci Eng* **94**, 77 (2006).
22. Simsek, E., Acatay, K. & Menciloglu, Y. Z. Effect of perfluoroacrylate ratio on the generation of stable superhydrophobic surfaces displaying low contact angle hysteresis. *Polym Prepr* **46(1)**, 385 (2005).
23. Acatay, K., Simsek, E., Ow-Yang, C. & Menciloglu, Y. Generation of superhydrophobic surfaces by electrospinning process. *Polym Prepr* **46(1)**, 399 (2005).
24. Ma, M. L., Mao, Y., Gupta, M., Gleason, K. K. & Rutledge, G. C. Superhydrophobic fabrics produced by electrospinning and chemical vapor deposition. *Macromolecules* **38**, 9742 (2005).
25. Ma, M. L., Hill, R. M., Lowery, J. L., Fridrikh, S. V. & Rutledge, G. C. Electrospun poly(styrene-block-dimethylsiloxane) block copolymer fibers exhibiting superhydrophobicity. *Langmuir* **21**, 5549 (2005).
26. Doshi, J. & Reneker, D. H. Electrospinning process and applications of electrospun fibers. *J Electrostat* **35**, 151 (1995).

27. Taylor, G. I. *Proceedings of the Royal Society of London A* **313**, 453 (1969).
28. Fong, H. & Reneker, H. R. *Structure Formation in Polymeric Fibers*, ed. D. R. Hanser Publications, Salem, Germany, 2001.
29. Deitzel, J. M., Kleinmeyer, J. D., Hirvonen, J. K. & Tan, N. C. B. Controlled deposition of electrospun poly(ethylene oxide) fibers. *Polymer* **42**, 8163 (2001).
30. Demir, M. M., Yilgor, I., Yilgor, E. & Erman, B. Electrospinning of polyurethane fibers. *Polymer* **43**, 3303 (2002).
31. Dettre, R. H. & Johnson Jr., R. E. Surface properties of polymers. I. Surface tensions of some molten polyethylenes. *J Colloid and Interface Sci* **21**, 367 (1966).
32. Dettre, R. H. & Johnson Jr., R. E. Surface tensions of perfluoroalkanes and poly(tetrafluoroethylene). *J Colloid and Interface Sci* **31**, 568 (1969).
33. Saidi, S., Guittard, F., Guimon, C. & Geribaldi, S. Low surface energy perfluorooctyl acrylate copolymers for surface modification of PET. *Macromol Chem Physic* **206**, 1098 (2005).
34. De Grampel, R. D. V., Ming, W., Gildenpfennig, A., van Gennip, W. J. H., Laven, J., Niemantsverdriet, J. W., Brongersma, H. H., de With, G. & van der Linde, R. The outermost atomic layer of thin films of fluorinated polymethacrylates. *Langmuir* **20**, 6344 (2004).
35. Tsibouklis, J., Stone, M., Thorpe, A. A., Graham, P., Nevell, T. G. & Ewen, R. J. Surface energy characteristics of polymer film structures: A further insight into the molecular design requirements. *Langmuir* **15**, 7076 (1999).
36. Saidi, S., Guittard, F., Guimon, C. & Geribaldi, S. Fluorinated acrylic polymers: Surface properties and XPS investigations. *J Appl Polym Sci* **99**, 821 (2006).
37. Park, I. J., Lee, S. B. & Choi, C. K. Surface properties of the fluorine-containing graft copolymer of poly((perfluoroalkyl)ethyl methacrylate)-g-poly(methyl methacrylate). *Macromolecules* **31**, 7555 (1998).
38. Wang, J. G., Mao, G. P., Ober, C. K. & Krammer, E. J. Liquid crystalline, semifluorinated side group block copolymers with stable low energy surfaces: Synthesis, liquid crystalline structure, and critical surface tension. *Macromolecules* **30**, 1906 (1997).
39. Tsibouklis, J. & Nevell, T. G. Ultra-low surface energy polymers: The molecular design requirements. *Adv Mater* **15**, 647 (2003).
40. Tsibouklis, J., Graham, P., Eaton, P. J., Smith, J. R., Nevell, T. G., Smart, J. D. & Ewen, R. J. Poly(perfluoroalkyl methacrylate) film structures: Surface organization phenomena, surface energy determinations, and force of adhesion measurements. *Macromolecules* **33**, 8460 (2000).

41. Graham, P., Stone, M., Thorpe, A., Nevell, T. G. & Tsibouklis, J. Fluoropolymers with very low surface energy characteristics. *J Fluorine Chem* **104**, 29 (2000).
42. Hayakawa, T., Wang, J. G., Xiang, M. L., Li, X. F., Ueda, M., Ober, C. K., Genzer, J., Sivaniah, E., Kramer, E. J. & Fischer, D. A. Effect of changing molecular end groups on surface properties: Synthesis and characterization of poly(styrene-*b*-semifluorinated isoprene) block copolymers with -CF<sub>2</sub>H end groups. *Macromolecules* **33**, 8012 (2000).
43. Wang, J. G. & Ober, C. K. Self-organizing materials with low surface energy: The synthesis and solid-state properties of semifluorinated side-chain ionenes. *Macromolecules* **30**, 7560 (1997).
44. Nishino, T., Urushihara, Y., Meguro, M. & Nakamae, K. Surface properties and structures of diblock and random copolymers with perfluoroalkyl side chains. *J Colloid Interf Sci* **279**, 364 (2004).
45. Adamson, A. W. & Gast, A. P. *Physical Chemistry of Surfaces*. Wiley-Interscience, New York, 1997.
46. Langmuir, I. Constitution and fundamental properties of solids and liquids. I. Solids. *J Am Chem Soc* **38**, 2221 (1916).
47. Li, X. F., Andruzzi, L., Chiellini, E., Galli, G., Ober, C. K., Hexemer, A., Kramer, E. J. & Fischer, D. A. Semifluorinated aromatic side-group polystyrene-based block copolymers: Bulk structure and surface orientation studies. *Macromolecules* **35**, 8078 (2002).
48. Genzer, J., Sivaniah, E., Kramer, E. J., Wang, J. G., Korner, H., Xiang, M. L., Char, K., Ober, C. K., DeKoven, B. M., Bubeck, R. A., Chaudhury, M. K., Sambasivan, S., and Fischer, D. A. The orientation of semifluorinated alkanes attached to polymers at the surface of polymer films. *Macromolecules* **33**, 1882 (2000).
49. Lafuma, A. & Quere, D. Superhydrophobic states. *Nat Mater* **2**, 457 (2003).
50. Owens, D. K. & Wendt, R. C. Estimation of the surface free energy of polymers. *J Appl Polym Sci* **13**, 1741 (1969).
51. Wu, S. *Polymer Interface and Adhesion*. Basel, New York, 1982.
52. Callewaert, M., Gohy, J. F., Dupont-Gillain, C. C., Boulange-Petermann, L. & Rouxhet, P. G. Surface morphology and wetting properties of surfaces coated with an amphiphilic diblock copolymer. *Surf Sci* **575**, 125 (2005).
53. Huh, C. & Mason, S. G. Effects of surface roughness on wetting (theoretical). *J Colloid Interf Sci* **60**, 11 (1977).

54. Extrand, C. W. Model for contact angles and hysteresis on rough and ultraphobic surfaces. *Langmuir* **18**, 7991 (2002).
55. Taniguchi, M. & Belfort, G. Correcting for surface roughness. Advancing and receding contact angles. *Langmuir* **18**, 6465 (2002).
56. Shuttleworth, R. & Bailey, G. L. J. Spreading of a liquid over a rough solid. *Dis Faraday Soc* **3**, 16 (1948).
57. Anastasiadis, S. H., Retsos, H., Pispas, S., Hadjichristidis, N. & Neophytides, S. Smart Polymer Surfaces. *Macromolecules* **36**, 1994 (2003).
58. Gao, L. C. & McCarthy, T. J. The "Lotus Effect" Explained: Two Reasons Why Two Length Scales of Topography Are Important. *Langmuir* **22**, 2966 (2006).
59. He, B., Patankar, N. A. & Lee, J. Multiple Equilibrium Droplet Shapes and Design Criterion for Rough Hydrophobic Surfaces. *Langmuir* **19**, 4999 (2003).
60. Patankar, N. A. On the Modeling of Hydrophobic Contact Angles on Rough Surfaces. *Langmuir* **19**, 1249 (2003).
61. Patankar, N. A. Mimicking the lotus effect: influence of double roughness structures and slender pillars. *Langmuir* **20**, 8209 (2004).